

## Stability and stabilization of the lattice Boltzmann method

R. A. Brownlee,\* A. N. Gorban, and J. Levesley

*Department of Mathematics, University of Leicester, Leicester LE1 7RH, United Kingdom*

(Received 3 November 2006; published 29 March 2007)

We revisit the classical stability versus accuracy dilemma for the lattice Boltzmann methods (LBM). Our goal is a stable method of second-order accuracy for fluid dynamics based on the lattice Bhatnager-Gross-Krook method (LBGK). The LBGK scheme can be recognized as a discrete dynamical system generated by free flight and entropic involution. In this framework the stability and accuracy analysis are more natural. We find the necessary and sufficient conditions for second-order accurate fluid dynamics modeling. In particular, it is proven that in order to guarantee second-order accuracy the distribution should belong to a distinguished surface—the invariant film (up to second order in the time step). This surface is the trajectory of the (quasi)equilibrium distribution surface under free flight. The main instability mechanisms are identified. The simplest recipes for stabilization add no artificial dissipation (up to second order) and provide second-order accuracy of the method. Two other prescriptions add some artificial dissipation locally and prevent the system from loss of positivity and local blowup. Demonstration of the proposed stable LBGK schemes are provided by the numerical simulation of a one-dimensional (1D) shock tube and the unsteady 2D flow around a square cylinder up to Reynolds number  $Re \sim 20\,000$ .

DOI: [10.1103/PhysRevE.75.036711](https://doi.org/10.1103/PhysRevE.75.036711)

PACS number(s): 47.11.-j

### I. INTRODUCTION

A lattice Boltzmann method (LBM) is a discrete velocity method in which a fluid is described by associating, with each velocity  $\mathbf{v}_i$ , a single-particle distribution function  $f_i = f_i(\mathbf{x}, t)$  which is evolved by advection and interaction on a fixed computational lattice. The method has been proposed as a discretization of Boltzmann's kinetic equation (for an introduction and historic review see [1]). Furthermore, the collision operator can be alluringly simplified, as is the case with the Bhatnager-Gross-Krook (BGK) operator [2], whereby collisions are described by a single-time relaxation to local equilibria  $f_i^*$ :

$$\frac{\partial f_i}{\partial t} + \mathbf{v}_i \cdot \nabla f_i = \frac{1}{\tau} (f_i^* - f_i) \quad (1)$$

The physically reasonable choice for  $f_i^*$  is as entropy maximizers, although other choices of equilibria are often preferred [1]. The local equilibria  $f_i^*$  depend nonlinearly on the hydrodynamic moments (density, momentum, etc.). These moments are linear functions of  $f_i$ , hence Eq. (1) is a nonlinear equation. For small  $\tau$ , the Chapman-Enskog approximation [3] reduces Eq. (1) to the compressible Navier-Stokes equation [1] with kinematic viscosity  $\nu = \frac{\tau}{2} c_1^2$ , where  $c_1$  is the thermal velocity for one degree of freedom.

The overrelaxation discretization of Eq. (1) (see, e.g., [1,4–8]) is known as the lattice Bhatnager-Gross-Krook method (LBGK), and allows one to choose a time step  $\delta_t \gg \tau$ . This decouples viscosity from the time step, thereby suggesting that LBGK is capable of operating at arbitrarily high-Reynolds number by making the relaxation time sufficiently small. However, in this low-viscosity regime, LBGK

suffers from numerical instabilities which readily manifest themselves as local blowups and spurious oscillations.

Another problem is the degree of accuracy. An approximation to the continuous-in-time kinetics is not equivalent to an approximation of the macroscopic transport equation. The fluid dynamics appears as a singular limit of the Boltzmann or BGK equation for small  $\tau$ . An approximation to the corresponding slow manifold in the distribution space is constructed by the Chapman-Enskog expansion. This is an asymptotic expansion, and higher (Burnett) terms could have singularities. An alternative approach to asymptotic expansion (with “diffusive scaling” instead of “convective scaling” in the Chapman-Enskog expansion) was developed in [9] in order to obtain the incompressible Navier-Stokes equations directly from kinetics.

It appears that the relaxation time of the overrelaxation scheme to the slow hydrodynamic manifold may be quite large for small viscosity:  $t_{\text{relax}} \simeq c_1^2 \delta_t^2 / (2\nu) = \delta_t^2 / \tau$  (see below, in Sec. III). Some estimates of long relaxation time for LBGK at large Reynolds number are found earlier in [10]. So, instead of fast relaxation to a slow manifold in continuous-in-time kinetics, we could meet a slow relaxation to a fluid dynamics manifold in the chain of discrete LBM steps.

Our approach is based on two ideas: the Ehrenfests' coarse graining [11–13] and the method of differential approximation of difference equations [14,15]. The background knowledge necessary to discuss the LBM in this manner is presented in Sec. II. In this section, we answer the question: how to provide second-order accuracy of the LBM methods for fluid dynamics modeling? We prove the necessary and sufficient conditions for this accuracy. It requires a special connection between the distribution  $f_i$  and the hydrodynamic variables. There is essentially one degree of freedom for the choice of  $f_i$ , if the hydrodynamic fields are given. Moreover, the LBM with overrelaxation can provide approximation of the macroscopic equation even when it does not approximate the continuous-in-time microscopic kinetics.

\*Corresponding author. Email address: [r.brownlee@mcs.le.ac.uk](mailto:r.brownlee@mcs.le.ac.uk)

This approach suggests several sources of numerical instabilities in the LBM and allows several recipes for stabilization. A geometric background for this analysis provides a manifold that is a trajectory  $\mathbf{q}$  of the quasiequilibrium manifold due to free flight. We call this manifold the *invariant film (of nonequilibrium states)*. It was introduced in [16] and studied further in [13,17,18]. Common to each stabilization recipe is the desire to stay uniformly close to the aforementioned manifold (Sec. III).

In Sec. IV, in addition to two LBM accuracy tests, a numerical simulation of a one-dimensional (1D) shock tube and the unsteady 2D flow around a square cylinder using the present stabilized LBM are presented. For the later problem, the simulation quantitatively validates the experimentally obtained Strouhal-Reynolds relationship up to  $\text{Re} \sim 20\,000$ . This extends previous LBM studies of this problem where the relationship had only been successfully validated up to  $\text{Re} \sim 5000$  [19,20].

Section V contains some concluding remarks as well as practical recommendations for LBM realization.

We use operator notation that allows us to present general results in compact form. The only definition we have to recall here is the (Gâteaux) differential: the differential of a map  $J(f)$  at a point  $f_0$  is a linear operator  $(D_f J)_{f_0}$  defined by a rule:  $(D_f J)_{f_0} g = d/d\varepsilon [J(f_0 + \varepsilon g)]_{\varepsilon=0}$ .

## II. BACKGROUND

### A. Microscopic and macroscopic variables

Let us describe the main elements of the LBM construction. The first element is a microscopic description, a single-particle distribution function  $f(\mathbf{x}, \mathbf{v})$ , where  $\mathbf{x}$  is the space vector and  $\mathbf{v}$  is velocity. If velocity space is approximated by a finite set  $\{\mathbf{v}_i\}$ , then the distribution is approximated by a measure with finite support,  $f(\mathbf{x}, \mathbf{v}) \simeq \sum_i f_i \delta(\mathbf{v} - \mathbf{v}_i)$ . In that case, the microscopic description is the finite-dimensional vector function  $f_i(\mathbf{x})$ .

The second main element is the macroscopic description. This is a set of macroscopic vector fields that are usually some moments of the distribution function. The main example gives the hydrodynamic fields (density-momentum-energy density):  $\{n, \mathbf{nu}, \mathcal{E}\}(\mathbf{x}) = \int \{1, \mathbf{v}, v^2/2\} f(\mathbf{x}, \mathbf{v}) d\mathbf{v}$ . But this is not an obligatory choice. If we would like to solve by LBM methods the Grad equations [21,22] or some extended thermodynamic equations [23], we should extend the list of moments (but, at the same time, we should be ready to introduce more discrete velocities for a proper description of these extended moment systems).

In general, we use the notation  $f$  for the microscopic state and  $M$  for the macroscopic state. The vector  $M$  is a linear function of  $f$ :  $M = m(f)$ .

### B. Equilibrium

For any allowable value of  $M$  an ‘‘equilibrium’’ distribution should be given: a microscopic state  $f_M^*$ . It should satisfy the obvious, but important identity of self-consistency,

$$m(f_M^*) = M, \quad (2)$$

or in differential form

$$m(D_M f_M^*) \equiv 1, \quad \text{i.e., } m((D_M f_M^*)a) \equiv a. \quad (3)$$

The state  $f_M^*$  is not a proper thermodynamic equilibrium, but a conditional one under the constraint  $m(f) = M$ . Therefore we call it a *quasiequilibrium* (other names, such as local equilibrium, conditional equilibrium, generalized canonical state, or pseudoequilibrium are also in use).

For the quasiequilibrium  $f_M^*$ , an equilibration operation is the projection  $\Pi^*$  of the distribution  $f$  into the corresponding quasiequilibrium state:  $\Pi^*(f) = f_{m(f)}^*$ .

In the fully physical situation with continuous velocity space, the quasiequilibrium  $f_M^*$  is defined as a conditional entropy maximizer by a solution of the optimization problem:

$$S(f) \rightarrow \max, \quad m(f) = M, \quad (4)$$

where  $S(f)$  is an entropy functional.

The choice of entropy is ambiguous; generally, we can start from a concave functional of the form

$$S(f) = \int s(f(\mathbf{x}, \mathbf{v}, t)) f(\mathbf{x}, \mathbf{v}, t) d\mathbf{x} d\mathbf{v}, \quad (5)$$

with a concave function of one variable  $s(f)$ . The choice by default is  $s(f) = -\ln f$ , which gives the classical Boltzmann-Gibbs-Shannon (BGS) entropy.

For discrete velocity space, there exist some extra moment conditions on the equilibrium construction: in addition to Eq. (2) some higher moments of a discrete equilibrium (fluxes) should be the same as for the continuous one. This is necessary to provide the proper macroscopic equations for  $M$ . Existence of entropy for the entropic equilibrium definition (4) while fulfilling higher moment conditions could be in contradiction, and a special choice of velocity set may be necessary (for a very recent example of such research for multispeed lattices see [24]). Another choice is to refuse to deal with the entropic definition of equilibrium (4) and assume that there will be no perpetuum mobile of the second kind. This extends the possibility for approximation, but creates some risk of nonphysical behavior of the model. For a detailed discussion of the  $H$  theorem for LBM we refer the readers to [25].

Some of the following results depend on the entropic definition of equilibrium, but some do not. We always point out if results are ‘‘entropy-free.’’

### C. Free flight

In the LBM construction the other main elements are the free-flight transformation and the collision. There are many models of collisions, but the free-flight equation is always the same,

$$\frac{\partial f}{\partial t} + \mathbf{v} \cdot \nabla_x f = 0, \quad (6)$$

with exact solution  $f(\mathbf{x}, \mathbf{v}, t) = f(\mathbf{x} - \mathbf{v}t, \mathbf{v}, 0)$ , or for discrete velocities,

$$\frac{\partial f_i}{\partial t} + \mathbf{v}_i \cdot \nabla_{\mathbf{x}} f_i = 0, \quad (7)$$

$f_i(\mathbf{x}, t) = f_i(\mathbf{x} - \mathbf{v}_i t, 0)$ . Free flight conserves any entropy of the form (5). In general, we can start from any dynamics. For application of the entropic formalism, this dynamics should conserve entropy. Let this kinetic equation be

$$\frac{df}{dt} = J_c(f). \quad (8)$$

For our considerations, the free-flight equation will be the main example of the conservative kinetics (8).

The phase flow  $\Theta_t$  for kinetic equation (8) is a shift in time that transforms  $f(t_0)$  into  $f(t_0 + t)$ . For free flight,  $\Theta_t: f(\mathbf{x}, \mathbf{v}) \rightarrow f(\mathbf{x} - \mathbf{v}t, \mathbf{v})$ .

*Remark.* We work with dynamical systems defined by partial differential equations. Strictly speaking, this means that the proper boundary conditions are fixed. In order to separate the discussion of equation from a boundary condition problem, let us imagine here a system with periodic boundary conditions (e.g., on a torus), or a system with equilibrium boundary conditions at infinity.

#### D. Ehrenfests' solver of second-order accuracy for the Navier-Stokes equations

Here we present a generalization of a well-known result. Let us study the following process (an example of the Ehrenfests' chain [11–13], a similar result gives the optimal prediction approach [26]): free flight for time  $\tau$ —equilibration—free flight for time  $\tau$ —equilibration—... During this process, the hydrodynamic fields approximate the solution of the (compressible) Navier-Stokes equation with viscosity  $\nu = \tau/2c_1^2$ , where  $c_1$  is the thermal velocity for one degree of freedom. The error of one step of this approximation has the order  $O(\tau^3)$ . An exact expression for the transport equation that is approximated by this process in the general situation (for arbitrary initial kinetics, velocity set, and for any set of moments) is

$$\frac{dM}{dt} = m(J_c(f_M^*)) + \frac{\tau}{2} m((D_{\mathbf{f}} J_c(f))_{f_M^*} \Delta_{f_M^*}), \quad (9)$$

where  $\Delta_{f_M^*}$  is the *defect of invariance* of the quasiequilibrium manifold

$$\Delta_{f_M^*} = J_c(f_M^*) - D_M(f_M^*)m(J_c(f_M^*)), \quad (10)$$

and is the difference between the vector field  $J_c$  and its projection on to the quasiequilibrium manifold. This result is entropy-free.

The first term in the right-hand side of Eq. (9)—the *quasiequilibrium approximation*—consists of moments of  $df/dt$  computed at the quasiequilibrium point. For free flight, hydrodynamic fields and Maxwell equilibria this term gives the Euler equations. The second term includes the action of the differential  $D_{\mathbf{f}} J_c(f)_{f_M^*}$  on the defect of invariance  $\Delta_{f_M^*}$  [for free flight (6), this differential is just  $-\mathbf{v} \cdot \nabla_{\mathbf{x}}$ , for the discrete version (7) this is the vector column  $-\mathbf{v}_i \cdot \nabla_{\mathbf{x}_i}$ ]. These terms always appear in the Chapman-Enskog expansion. For free

flight, hydrodynamic fields, and Maxwell equilibria they give the Navier-Stokes equations for a monoatomic gas with Prandtl number  $\text{Pr} = 1$ :

$$\begin{aligned} \frac{\partial n}{\partial t} &= - \sum_i \frac{\partial(nu_i)}{\partial x_i}, \\ \frac{\partial(nu_k)}{\partial t} &= - \sum_i \frac{\partial(nu_k u_i)}{\partial x_i} - \frac{1}{m} \frac{\partial P}{\partial x_k} \\ &\quad + \frac{\tau}{2m} \sum_i \frac{\partial}{\partial x_i} \left[ P \left( \frac{\partial u_k}{\partial x_i} + \frac{\partial u_i}{\partial x_k} - \frac{2}{3} \delta_{ki} \text{div } u \right) \right], \\ \frac{\partial \mathcal{E}}{\partial t} &= - \sum_i \frac{\partial(\mathcal{E}u_i)}{\partial x_i} - \frac{1}{m} \sum_i \frac{\partial(Pu_i)}{\partial x_i} + \frac{\tau}{2} \frac{5k_B}{2m^2} \sum_i \frac{\partial}{\partial x_i} \left( P \frac{\partial T}{\partial x_i} \right), \end{aligned} \quad (11)$$

where  $m$  is particle mass,  $k_B$  is Boltzmann's constant,  $P = nk_B T$  is ideal gas pressure,  $T$  is kinetic temperature, and the underlined terms are the results of the coarse graining additional to the quasiequilibrium approximation.

All computations are straightforward exercises (differential calculus and Gaussian integrals for computation of the moments,  $m$ , in the continuous case). More details of these computations are presented in [18].

The dynamic viscosity in (11) is  $\mu = \frac{\tau}{2} nk_B T$ . It is useful to compare this formula to the mean-free-path theory that gives  $\mu = \tau_{\text{col}} nk_B T$ , where  $\tau_{\text{col}}$  is the collision time (the time for the mean-free path). According to these formulas, we obtain the following interpretation of the coarse-graining time  $\tau$  for this example:  $\tau = 2\tau_{\text{col}}$ .

For any particular choice of discrete velocity set  $\{\mathbf{v}_i\}$  and of equilibrium  $f_M^*$  the calculation could give different equations, but the general formula (9) remains the same. The connection between discretization and viscosity was also studied in [27]. Let us prove the general formula (9).

We are looking for a macroscopic system that is approximated by the Ehrenfests' chain. Let us look for macroscopic equations of the form

$$\frac{dM}{dt} = \Psi(M), \quad (12)$$

with the phase flow  $\Phi_t: M(t) = \Phi_t M(0)$ . The transformation  $\Phi_\tau$  should coincide with the transformation  $M \mapsto m(\Theta_\tau(f_M^*))$  up to second order in  $\tau$ . The matching condition is

$$m(\Theta_\tau(f_M^*)) = \Phi_\tau(M) \quad \text{for every } M \text{ and given } \tau. \quad (13)$$

This condition is the equation for the macroscopic vector field  $\Psi(M)$ . The solution of this equation is a function of  $\tau$ :  $\Psi = \Psi(M, \tau)$ . For a sufficiently smooth microscopic vector field  $J_c(f)$  and entropy  $S(f)$  it is easy to find the Taylor expansion of  $\Psi(M, \tau)$  in powers of  $\tau$ . Let us find the first two terms:  $\Psi(M, \tau) = \Psi_0(M) + \tau \Psi_1(M) + o(\tau)$ . Up to second order in  $\tau$  the matching condition (13) is

$$\begin{aligned}
& m(J_c(f_M^*))\tau + m((D_f J_c(f))_{f_M^*}(J_c(f_M^*)))\frac{\tau^2}{2} \\
&= \Psi_0(M)\tau + \Psi_1(M)\tau^2 + (D_M \Psi_0(M))(\Psi_0(M))\frac{\tau^2}{2}.
\end{aligned} \tag{14}$$

From this condition immediately follows

$$\begin{aligned}
\Psi_0(M) &= m(J_c(f_M^*)), \\
\Psi_1(M) &= \frac{1}{2}m((D_f J_c(f))_{f_M^*}\Delta_{f_M^*}),
\end{aligned} \tag{15}$$

where  $\Delta_{f_M^*}$  is the defect of invariance (10). Thus we find that the macroscopic equation in the first approximation is Eq. (9).

### E. The Chapman-Enskog expansion for the generalized Bhatnager-Gross-Krook equation

Here we present the Chapman-Enskog method for a class of generalized model equations. This class includes the well-known BGK kinetic equation, as well as many other model equations [28].

As a starting point we take a formal kinetic equation with a small parameter  $\tau$ ,

$$\frac{df}{dt} = J(f) := J_c(f) + \frac{1}{\tau}[\Pi^*(f) - f]. \tag{16}$$

The term  $\Pi^*(f) - f$  is nonlinear because of the nonlinear dependency of  $\Pi^*(f) = f_{m(f)}^*$  on  $m(f)$ .

We would like to find a reduced description valid for the macroscopic variables  $M$ . This means, at least, that we are looking for an invariant manifold parametrized by  $M$ ,  $f = f_M$ , that satisfies the *invariance equation*

$$(D_M f_M)(m(J(f_M))) = J(f_M). \tag{17}$$

The invariance equation means that the time derivative of  $f$  calculated through the time derivative of  $M$  ( $\dot{M} = m(J(f_M))$ ) by the chain rule coincides with the true time derivative  $J(f)$ . This is the central equation for model reduction theory and applications. The first general results about existence and regularity of solutions to Eq. (17) were obtained by Lyapunov [29] (see, e.g., the review in [18]). For the kinetic equation (16) the invariance equation has the form

$$(D_M f_M)(m(J_c(f_M))) = J_c(f_M) + \frac{1}{\tau}(f_M^* - f_M), \tag{18}$$

because of the self-consistency identity (2) and (3).

Due to the presence of the small parameter  $\tau$  in  $J(f)$ , the zero approximation to  $f_M$  is the quasiequilibrium approximation:  $f_M^{(0)} = f_M^*$ . Let us look for  $f_M$  in the form of a power series:  $f_M = f_M^{(0)} + \tau f_M^{(1)} + \dots$ , with  $m(f_M^{(k)}) = 0$  for  $k \geq 1$ . From Eq. (18) we immediately find

$$f_M^{(1)} = J_c(f_M^{(0)}) - (D_M f_M^{(0)})(m(J_c(f_M^{(0)}))) = \Delta_{f_M^*}. \tag{19}$$

It is very natural that the first term of the Chapman-Enskog expansion for the model equation (16) is just the defect of invariance for the quasiequilibrium (10).

The corresponding first order in  $\tau$  approximation for the macroscopic equations is

$$\frac{dM}{dt} = m(J_c(f_M^*)) + \tau m((D_f J_c(f))_{f_M^*}\Delta_{f_M^*}). \tag{20}$$

We should recall that  $m(\Delta_{f_M^*}) = 0$ . The last term in Eq. (18) vanishes in the macroscopic projection for all orders. The only difference between Eq. (20) and Eq. (9) is the coefficient  $1/2$  before  $\tau$  in Eq. (9).

### F. Decoupling of time step and viscosity: how to provide second-order accuracy

In the Ehrenfests' chain "free flight—equilibration—..." the starting point of each link is a quasiequilibrium state: the chain starts from  $f_{M(0)}^*$ , then, after free flight, equilibrates into  $f_{M(\tau)}^*$ , etc. The viscosity coefficient in Eq. (9) is proportional to  $\tau$ . Let us choose another starting point ( $f_M^*$ ) in order to decouple time step and viscosity and preserve the second-order accuracy of approximation. We would like to obtain Eq. (9) with a chain time step  $\delta_t = h$ . Analogously to Eqs. (14) and (15), we obtain the macroscopic equation

$$\frac{dM}{dt} = m(J_c(f_M^*)) + m((D_f J_c(f))_{f_M^*}[(f_M^s - f_M^*) + (h/2)\Delta_{f_M^*}]), \tag{21}$$

under the condition that  $f_M^s - f_M^* = O(h)$ . The initial point

$$f_M^s = f_M^* - \frac{1}{2}(h - \tau)\Delta_{f_M^*} + o(h) \tag{22}$$

provides the required viscosity. This is a sufficient condition for the second-order accuracy of the approximation. Of course, the self-consistency identity  $m(f_M^s) = M$  should be valid exactly, as Eq. (2) is. This starting distribution is a linear combination of the quasiequilibrium state and the first Chapman-Enskog approximation.

The necessary and sufficient condition for second-order accuracy of the approximation is

$$m((D_f J_c(f))_{f_M^*}[f_M^s - f_M^* + \frac{1}{2}(h - \tau)\Delta_{f_M^*}]) = o(h) \tag{23}$$

[with the self-consistency identity  $m(f_M^s) = M$ ]. This means that the difference between left- and right-hand sides of Eq. (22) should have zero moments and give zero inputs in observable macroscopic fluxes.

Hence, the condition of second-order accuracy significantly restricts the possible initial point for free flight. This result is also entropy-free.

Any construction of collisions should keep the system's starting free-flight steps near the points  $f_M^s$  given by Eqs. (22) and (23). The conditions (22) and (23) for second-order accuracy of the transport equation approximation do not de-

pend on a specific collision model, they are valid for most modifications of the LBM and LBGK that use free flight as a main step.

Various multistep approximations give more freedom of choice for the initial state. For the construction of such approximations below, the following *mean viscosity lemma* is important: if the transformations  $\Omega_i^h: M \rightarrow M'$ ,  $i=1, \dots, k$ , approximate the phase flow for Eq. (9) for time  $h$  (shift in time  $h$ ) and  $\tau = \tau_i$  with second-order accuracy in  $h$ , then the superposition  $\Omega_1^h \Omega_2^h \dots \Omega_k^h$  approximates the phase flow for Eq. (9) for time  $kh$  (shift in time  $kh$ ) for the average viscosity  $\tau = \frac{1}{k}(\tau_1 + \dots + \tau_k)$  with the same order of accuracy. The proof is by straightforward multiple applications of Taylor's formula.

### G. Entropic formula for $D_M(f_M^*)$

Among the many benefits of thermodynamics for stability analysis there are some technical issues, too. The differential of equilibrium  $D_M(f_M^*)$  appears in many expressions, for example, Eqs. (3), (10), (14), (15), (17), and (18). If the quasiequilibrium is defined by the solution of the optimization problem (4), then

$$D_M f_M^* = (D_f^2 S)_{f_M^*}^{-1} m^T (m (D_f^2 S)_{f_M^*}^{-1} m^T)^{-1}. \quad (24)$$

This operator is constructed from the vector  $m$ , the transposed vector  $m^T$ , and the second differential of entropy. The inverse Hessian  $(\partial^2 S / \partial f_i \partial f_j)^{-1}$  is especially simple for the BGS entropy, it is just  $f_i \delta_{ij}$ . The formula (24) was first obtained in [30] (for an important particular case; for further references see [18]).

### H. Invariant film

All the points  $\Theta_t(f_M^*)$  belong to a manifold that is a trajectory  $\mathbf{q}$  of the quasiequilibrium manifold due to the conservative dynamics (8) [in hydrodynamic applications this is the free-flight dynamics (6)]. We call this manifold the *invariant film (of nonequilibrium states)*. It was introduced in [16] and studied further in [13,17,18]. The defect of invariance  $\Delta_{f_M^*}$  (10) is tangent to  $\mathbf{q}$  at the point  $f_M^*$ , and belongs to the intersection of this tangent space with  $\ker m$ . This intersection is one dimensional. This means that the direction of  $\Delta_{f_M^*}$  is selected from the tangent space to  $\mathbf{q}$  by the condition: derivative of  $M$  in this direction is zero.

A point  $f$  on the invariant film  $\mathbf{q}$  is naturally parametrized by  $(M, t)$ :  $f = q_{M,t}$ , where  $M = m(f)$  is the value of the macroscopic variables and  $t = t(f)$  is the time shift from a quasiequilibrium state;  $\Theta_{-t}(f)$  is a quasiequilibrium state for some (other) value of  $M$ . By definition, the action of  $\Theta_t$  on the second coordinate of  $q_{M,t}$  is simple:  $\Theta_t(q_{M,t}) = q_{M',t+\tau}$ . To the first order in  $t$ ,

$$q_{M,t} = f_M^* + t \Delta_{f_M^*} \quad (25)$$

and  $q_{M,0} \equiv f_M^*$ . The quasiequilibrium manifold divides  $\mathbf{q}$  into two parts,  $\mathbf{q} = \mathbf{q}_- \cup \mathbf{q}_0 \cup \mathbf{q}_+$ , where  $\mathbf{q}_- = \{q_{M,t} | t < 0\}$ ,  $\mathbf{q}_+ = \{q_{M,t} | t > 0\}$ , and  $\mathbf{q}_0$  is the quasiequilibrium manifold:  $\mathbf{q}_0 = \{q_{M,0}\} = \{f_M^*\}$ .

There is an important *temporal involution* of the film,

$$I_T(q_{M,t}) = q_{M,-t}. \quad (26)$$

Due to Eq. (22), for  $q_{M,t}$  and a given time step  $h$  the transformation  $M \mapsto m(\Theta_h(q_{M,t}))$  approximates the solution of Eq. (9) with  $\tau = 2t + h$  for the initial conditions  $M$  and time step  $h$  with second-order accuracy in  $h$ . Hence, due to the mean viscosity lemma, the two-step transformation

$$M \mapsto m(I_T(\Theta_h(I_T(\Theta_h(q_{M,t})))))) \quad (27)$$

approximates the solution of Eq. (9) with  $\tau = 0$  (the Euler equations) for the initial conditions  $M$  and time step  $h$  with second-order accuracy in  $h$ . This is true for any  $t$ , hence, for any starting point on the invariant film with the given value of  $M$ .

To approximate the solution of Eq. (9) with nonzero  $\tau$ , we need an ‘‘incomplete involution,’’

$$I_T^\beta(q_{M,t}) = q_{M, -(2\beta-1)t}. \quad (28)$$

For  $\beta = 1$ , we have  $I_T^\beta = I_T$  and for  $\beta = 1/2$ ,  $I_T^{1/2}$  is just the projection onto the quasiequilibrium manifold:  $I_T^{1/2}(q_{M,t}) = \Pi^*(q_{M,t}) = q_{M,0}$ . After some initial steps, the following sequence gives a second order in time step  $h$  approximation of Eq. (9) with  $\tau = (1 - \beta)h/\beta$ ,  $1/2 \leq \beta \leq 1$ :

$$M_n = m((I_T^\beta \Theta_h)^n q_{M,t}). \quad (29)$$

To prove this statement we consider a transformation of the second coordinate in  $q_{M,\vartheta_n}$  by  $I_T^\beta \Theta_h$ ,

$$\vartheta_{n+1} = -(2\beta - 1)(\vartheta_n + h). \quad (30)$$

This transformation has a fixed point  $\vartheta^* = -h(2\beta - 1)/(2\beta)$  and  $\vartheta_n = \vartheta^* + (-1)^n(2\beta - 1)^n \delta$  for some  $\delta$ . If  $1 - \beta$  is small then relaxation may be very slow:  $\vartheta_n \approx \vartheta^* + (-1)^n \delta \exp[-2n(1 - \beta)]$ , and relaxation requires  $\approx 1/[2(1 - \beta)]$  steps. If  $\vartheta_n = \vartheta^* + o(h)$  then the sequence  $M_n$  (29) approximates Eq. (9) with  $\tau = h - 2|\vartheta^*| = (1 - \beta)h/\beta$  and second-order accuracy in the time step  $h$ . The fixed points  $q_{M,\vartheta^*}$  coincide with the restart points  $f_M^* + \vartheta^* \Delta_{f_M^*}$  (22) in the first order in  $\vartheta^* = -(h - \tau)/2$ , and the middle points  $\vartheta^* + h/2$  of the free-flight jumps  $q_{M,\vartheta^*} \mapsto q_{M',\vartheta^*+h}$  approximate the first-order Chapman-Enskog manifold  $f_M^* + \frac{\tau}{2} \Delta_{f_M^*}$ .

For the entropic description of quasiequilibrium, we can connect time with entropy and introduce entropic coordinates. For each  $M$  and positive  $s$  from some interval  $0 < s < \varsigma$  there exist two numbers  $t_\pm(M, s)$  [ $t_+(M, s) > 0$ ,  $t_-(M, s) < 0$ ] such that

$$S(q_{M,t_\pm(M,s)}) = S(f_M^*) - s. \quad (31)$$

The numbers  $t_\pm$  coincide to the first order  $t_+ = -t_- + o(t_-)$ .

We define the *entropic involution*  $I_S$  as a transformation of  $\mathbf{q}$ ,

$$I_S(q_{M,t_\pm}) = q_{M,t_\mp}. \quad (32)$$

The introduction of ‘‘incomplete entropic involution’’  $I_S^\beta$  is also obvious (see [13]).

Entropic involution  $I_S$  coincides with the temporal involution  $I_T$ , up to second order in the deviation from quasiequi-

librium state  $f - \Pi^*(f)$ . Hence, in the vicinity of quasiequilibrium there is no significant difference between these operations, and all statements about the temporal involution are valid for the entropic involution with the same level of accuracy.

For the transfer from free flight with temporal or entropic involution to the standard LBGK models we must transfer from dynamics and involution on  $\mathbf{q}$  to the whole space of states. Instead of  $I_T^\beta$  or  $I_S^\beta$  the transformation

$$I_0^\beta: f \mapsto \Pi^*(f) + (2\beta - 1)[\Pi^*(f) - f] \quad (33)$$

is used. For  $\beta=1$ ,  $I_0^1$  is a mirror reflection in the quasiequilibrium state  $\Pi^*(f)$ , and for  $\beta=1/2$ ,  $I_0^{1/2}$  is the projection onto the quasiequilibrium manifold. If, for a given  $f_0=q_{M,t}$ , the sequence (29) gives a second order in time step  $h$  approximation of Eq. (9), then the sequence

$$M_n = m((I_0^\beta \Theta_h)^n f_0) \quad (34)$$

also gives a second-order approximation to the same equation with  $\tau=(1-\beta)h/\beta$ . This chain is the standard LBGK model.

Entropic LBGK (ELBGK) methods [13,25,31,32] differ only in the definition of Eq. (33): for  $\beta=1$  it should conserve entropy, and in general has the form

$$I_E^\beta(f) = (1-\beta)f + \beta\tilde{f}, \quad (35)$$

with  $\tilde{f}=(1-\alpha)f + \alpha\Pi^*(f)$ . The number  $\alpha=\alpha(f)$  is chosen so that a constant entropy condition is satisfied,  $S(f)=S(\tilde{f})$ . For LBGK (33),  $\alpha=2$ .

Of course, computation of  $I_0^\beta$  is much easier than that of  $I_T^\beta$ ,  $I_S^\beta$ , or  $I_E^\beta$ : it is not necessary to follow exactly the manifold  $\mathbf{q}$  and to solve the nonlinear constant entropy condition equation. For an appropriate initial condition from  $\mathbf{q}$  (not sufficiently close to  $\mathbf{q}_0$ ), two steps of LBGK with  $I_0^\beta$  give the same second-order accuracy as Eq. (29). But a long chain of such steps can lead far from the quasiequilibrium manifold and even from  $\mathbf{q}$ . Here, we see stability problems arising. For  $\beta$  close to 1, the one-step transformation  $I_0^\beta \Theta_h$  in the chain (34) almost conserves distances between microscopic distributions, hence, we cannot expect fast exponential decay of any mode, and this system is near the boundary of Lyapunov stability.

### I. Does lattice Bhatnagar-Gross-Krook method with overrelaxation collisions approximate the Bhatnagar-Gross-Krook equation?

The BGK equation as well as its discrete velocity version (1) has a direction of fast contraction  $\Pi^*(f)-f$ . The discrete chain (34) with  $\beta$  close to 1 has nothing similar. Hence, the approximation of a genuine BGK solution by an LBGK chain may be possible only if both the BGK and the LBGK chain trajectories belong to a slow manifold with high accuracy. This implies significant restrictions on initial data and on the dynamics of the approximated solution, as well as fast relaxation of the LBGK chain to the slow manifold.

The usual Taylor-series-based arguments from [33] are valid for  $h \ll \tau$ . If we assume  $h \gg \tau$  ( $\delta_i \gg \lambda$  in the notation of

[33]), then Eq. (10) of [33] transforms (in our notation) into  $f(\mathbf{x}+\mathbf{v}h, \mathbf{v}, t+h) = f_M^*(\mathbf{x}+\mathbf{v}h, \mathbf{v}, t+h) + O(\tau)$  with  $M=m(f(\mathbf{x}+\mathbf{v}h, \mathbf{v}, t+h))$ . That is,  $f(\mathbf{x}, \mathbf{v}, t+h) = f_M^*(\mathbf{x}, \mathbf{v}, t+h) + O(\tau)$ . According to this formula,  $f$  should almost be at quasiequilibrium after a time step  $h \gg \tau$ , with some correction terms of order  $\tau$ . This first order in  $\tau$  correction is, of course, the first term of the Chapman-Enskog expansion (19):  $\tau f_M^{(1)} = \tau \Delta_{\mathbf{v}} f_M^*$  [with possible error of order  $O(\tau h)$ ]. This is a very natural result for an approximation of the BGK solution, especially in light of the Chapman-Enskog expansion [3,33], but it is not the LBM scheme with overrelaxation.

The standard element in the proof of second-order accuracy of the BGK equation approximation by an LBGK chain uses the estimation of an integral: for time step  $h$  we obtain from Eq. (1) the exact identity

$$f_i(\mathbf{x} + \mathbf{v}_i h, t+h) = \frac{1}{\tau} \int_t^{t+h} [f_{i,m(f)}^*(\mathbf{x}) - f_i(\mathbf{x}, t')] dt', \quad (36)$$

where  $f_{i,m(f)}^*(\mathbf{x})$  is the quasiequilibrium state that corresponds to the hydrodynamic fields  $m(f(\mathbf{x}, t'))$ . Then one could apply the trapezoid rule for integration to the right-hand side of Eq. (36). The error of the trapezoid rule has the order  $O(h^3)$ :

$$\int_t^{t+h} Q(t') dt' = \frac{h}{2} [Q(t) + Q(t+h)] - \frac{h^3}{12} \ddot{Q}(t'),$$

where  $t' \in [t, t+h]$  is *a priori* unknown point. But for the singularly perturbed system (1), the second derivative of the term  $f_{i,m(f)}^*(\mathbf{x}) - f_i(\mathbf{x}, t')$  on the right-hand side of Eq. (36) could be of order  $1/\tau^2$ , and the whole error estimate is  $O(h^3/\tau^3)$ . This is not small for  $h > \tau$ . For backward or forward in time estimates of the integral (36), errors have the order  $O(h^2/\tau^2)$ . Hence, for overrelaxation with  $h \gg \tau$  this reasoning is not applicable. Many simple examples of quantitative and qualitative errors of this approximation for a singularly perturbed system could be obtained by analysis of a simple system of two equations:  $\dot{x} = \frac{1}{\tau}[\phi(y) - x]$ ,  $\dot{y} = \psi(x, y)$  for various  $\phi$  and  $\psi$ . There are examples of slow relaxation (instead of fast), of blowup instead of relaxation, or of spurious oscillations, etc.

Hence, one cannot state that LBGK with overrelaxation collisions and  $\delta t \geq \tau$  approximates solutions of the BGK equation. Nevertheless, it can do another job: it can approximate solutions of the macroscopic transport equation. As demonstrated within this section, the LBGK chain (34), after some initial relaxation period, provides a second-order approximation to the transport equation, if it goes close to the invariant film up to the order  $O(h^2)$  [this initial relaxation period may have the order  $O(h^2/\tau)$ ]. In other words, it gives the required second-order approximation for the macroscopic transport equation under some stability conditions.

## III. STABILITY AND STABILIZATION

### A. Instabilities

Many definitions of stability, from Lagrange to Lyapunov, are based on the consideration of positively invariant vicini-

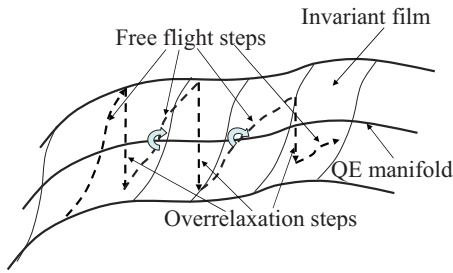


FIG. 1. (Color online) Directional instability: after several iterations the trajectory is not tangent to the invariant film with the required accuracy.

ties of solutions. Such a vicinity  $V$  is a “bag” for solutions: any solution belonging to  $V$  at some time  $t_0$  belongs to  $V$  for all  $t > t_0$ . Lagrange stability deals with one such bag, whereas Lyapunov stability of a solution requires a basis of such vicinities (see, e.g., [29,34,35]). From this point of view, the positivity condition, or the bounded total variation requirement are particular cases of stability conditions. The full consideration of all reasonable stability definitions is not our goal, and below we qualitatively discuss issues that are most important for our construction.

1. Positivity loss

First of all, if  $f$  is far from the quasiequilibrium, the positivity conditions (positivity of probabilities or populations) may be violated. For multidimensional and infinite-dimensional problems it is necessary to specify what one means by *far*. In the previous section,  $f$  is the whole state which includes the states of all sites of the lattice. All the involution operators with classical entropies are defined for lattice sites independently. Violation of positivity at one site makes the whole state nonphysical. Hence, we should use here the  $\ell_\infty$  norm: close states are close uniformly, at all sites.

Of course, violation of positivity of populations (a microscopic condition), does not affect the macroscopic motion immediately. For example, microscopic positivity is a sufficient, but not necessary condition for macroscopic positivity. This sufficient condition is convenient for control and for construction of limiters that guarantee macroscopic positivity and improve stability (see [36,37] and below).

2. Large deviations

The second problem is nonlinearity: for accuracy estimates we always use the assumption that  $f$  is sufficiently close to quasiequilibrium. Far from the quasiequilibrium manifold these estimates do not work because of nonlinearity (first of all, the quasiequilibrium distribution,  $f_M^*$ , depends nonlinearly on  $M$  and hence the projection operator,  $\Pi^*$ , is nonlinear). Again we need to keep the states not far from the quasiequilibrium manifold.

3. Directional instability

The third problem is a directional instability that can affect accuracy: the vector  $f - \Pi^*(f)$  can deviate far from the tangent to  $\mathbf{q}$  (Fig. 1). Hence, we should not only keep  $f$  close

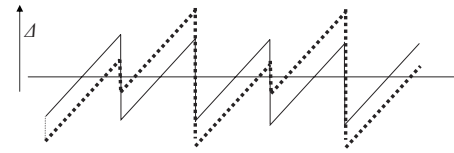


FIG. 2. Neutral stability and two-step oscillations in a sequence of reflections. Bold dotted line—a perturbed motion;  $\Delta$ —direction of neutral stability.

to the quasiequilibrium, but also guarantee smallness of the angle between the direction  $f - \Pi^*(f)$  and tangent space to  $\mathbf{q}$ .

One could rely on the stability of this direction, but we fail to prove this in any general case. The directional instability changes the structure of dissipation terms: the accuracy decreases to the first order in time step  $h$  and significant fluctuations of the Prandtl number and viscosity, etc. may occur. This carries a danger even without blowups; one could conceivably be relying on nonreliable computational results.

4. Direction of neutral stability

Further, there exists a neutral stability of all described approximations that causes two-step oscillations: a small shift of  $f$  in the direction of  $\Delta_{f_M^*}$  does not relax back for  $\beta = 1$ , and its relaxation is slow for  $\beta \approx 1$  (for small viscosity). This effect is demonstrated for a chain of mirror reflections in Fig. 2. There may be large deviation from the regular overrelaxation “zigzag.”

B. Dissipative recipes for stabilization

1. Positivity rule

There is a simple recipe for positivity preservation [37,38]: to substitute nonpositive  $I_0^\beta(f)(\mathbf{x})$  by the closest non-negative state that belongs to the straight line

$$\{\lambda f(\mathbf{x}) + (1 - \lambda)\Pi^*(f(\mathbf{x})) | \lambda \in \mathbb{R}\} \quad (37)$$

defined by the two points,  $f(\mathbf{x})$  and its corresponding quasiequilibrium state. This operation is to be applied pointwise, at the points of the lattice where the positivity is violated. The coefficient  $\lambda$  depends on  $\mathbf{x}$ , too. Let us call this recipe the *positivity rule* (Fig. 3); it preserves positivity of populations and probabilities, but can affect the accuracy of approximation. The same rule is necessary for ELBGK (35) when a positive “mirror state”  $\tilde{f}$  with the same entropy as  $f$  does not exist on the straight line (37).

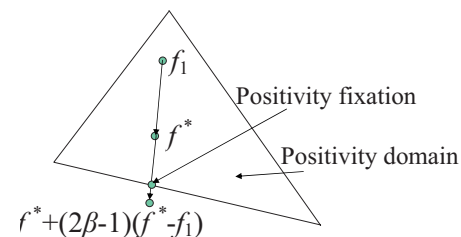


FIG. 3. (Color online) Positivity rule in action. The motions stops at the positivity boundary.

The positivity rule saves the existence of positive solutions, but affects dissipation because the result of the adjusted collision is closer to quasiequilibrium. There is a family of methods that modify collisions at some points by additional shift in the direction of quasiequilibrium. The positivity rule represents the minimal necessary modification. It is reasonable to always use this rule for LBM (as a “salvation rule”).

### 2. Ehrenfests’ regularization

To discuss methods with additional dissipation, the entropic approach is very convenient. Let entropy  $S(f)$  be defined for each population vector  $f=(f_i)$  (below, we use the same letter  $S$  for local-in-space entropy, and hope that the context will make this notation clear). We assume that the global entropy is a sum of local entropies for all sites. The local nonequilibrium entropy is

$$\Delta S(f) = S(f^*) - S(f), \quad (38)$$

where  $f^*$  is the corresponding local quasiequilibrium at the same point.

The *Ehrenfests’ regularization* [36,38] provides “entropy trimming:” we monitor local deviation of  $f$  from the corresponding quasiequilibrium, and when  $\Delta S(f, \mathbf{x})$  exceeds a pre-specified threshold value  $\delta$ , perform local Ehrenfests’ steps to the corresponding equilibrium. So that the Ehrenfests’ steps are not allowed to degrade the accuracy of LBGK it is pertinent to select the  $k$  sites with highest  $\Delta S > \delta$ . The *a posteriori* estimates of added dissipation could easily be performed by analysis of entropy production in Ehrenfests’ steps. Numerical experiments show (see, e.g., [36,38] and Sec. IV) that even a small number of such steps drastically improves stability.

To avoid the change of accuracy order “on average,” the number of sites with this step should be  $O(N\delta_x/L)$  where  $N$  is the total number of sites,  $\delta_x$  is the step of the space discretization, and  $L$  is the macroscopic characteristic length. But this rough estimate of accuracy in average might be destroyed by concentrations of Ehrenfests’ steps in the most nonequilibrium areas, for example, in boundary layers. In that case, instead of the total number of sites  $N$  in the estimate  $O(N\delta_x/L)$  we should take the number of sites in a specific region [60]. The effects of concentration could be easily analyzed *a posteriori*.

### 3. Entropic steps for nonentropic equilibria

If the approximate discrete equilibrium  $f^*$  is nonentropic, we can use  $\Delta S_K(f) = -S_K(f)$  instead of  $\Delta S(f)$ , where  $S_K$  is the Kullback entropy. This entropy,

$$S_K(f) = - \sum_i f_i \ln \left( \frac{f_i}{f_i^*} \right), \quad (39)$$

gives the physically reasonable entropic distance from equilibrium, if the supposed continuum system has the classical BGS entropy. In thermodynamics, the Kullback entropy belongs to the family of Massieu-Planck-Kramers functions (canonical or grand canonical potentials). One can use Eq.

(39) in the construction of Ehrenfests’ regularization for any choice of discrete equilibrium.

We have introduced two procedures: the positivity rule and Ehrenfests’ regularization. Both improve stability, reduce nonequilibrium entropy, and, hence, nonequilibrium fluxes. The proper context for discussion of such procedures are the flux limiters in finite difference and finite volume methods. Here we refer to the classical flux-corrected transport (FCT) algorithm [39] that strictly maintains positivity, and to its further developments [40–42].

### 4. Smooth limiters of nonequilibrium entropy

The positivity rule and Ehrenfests’ regularization provide rare, intense, and localized corrections. Of course, it is easy and also computationally cheap to organize more gentle transformations with smooth shifts of higher nonequilibrium states to equilibrium. The following regularization transformation distributes its action smoothly:

$$f \mapsto f^* + \phi(\Delta S(f))(f - f^*). \quad (40)$$

The choice of the function  $\phi$  is highly ambiguous, for example,  $\phi = 1/(1 + \alpha\Delta S^k)$  for some  $\alpha > 0$ ,  $k > 0$ . There are two significantly different choices: (i) ensemble-independent  $\phi$  (i.e., the value of  $\phi$  depends on the local value of  $\Delta S$  only) and (ii) ensemble-dependent  $\phi$ , for example,

$$\phi = \frac{1 + [\Delta S/(\alpha E(\Delta S))]^{k-1/2}}{1 + [\Delta S/(\alpha E(\Delta S))]^k},$$

where  $E(\Delta S)$  is the average value of  $\Delta S$  in the computational area,  $k \geq 1$  and  $\alpha \geq 1$ . It is easy to select an ensemble-dependent  $\phi$  with control of total additional dissipation.

### 5. Entropic lattice Bhatnager-Gross-Krook collisions as a smooth limiter

On the basis on numerical tests, the authors of [37] claim that the positivity rule provides the same results (in the sense of stability and absence and/or presence of spurious oscillations) as the ELBGK models, but ELBGK provides better accuracy.

For the formal definition of ELBGK (35) our tests do not support claims that ELBGK erases spurious oscillations (see Sec. IV below). Similar observations for Burgers equation has been reported in [43]. We understand this situation in the following way. The entropic method consists of at least three components: (1) entropic quasiequilibrium defined by entropy maximization; (2) entropy balanced collisions (35) that have to provide proper entropy balance; (3) a method for the solution of the transcendental equation  $S(f) = S(\tilde{f})$  to find  $\alpha = \alpha(f)$  in (35). It appears that the first two items do not affect spurious oscillations at all, if we solve the equation for  $\alpha(f)$  with high accuracy. Additional viscosity could, potentially, be added by use of explicit analytic formulas for  $\alpha(f)$ . In order not to decrease entropy, the errors in these formulas always increase dissipation. This can be interpreted as a hidden transformation of the form (40), where the coefficients of  $\phi$  also depend on  $f^*$ .

Compared to flux limiters, nonequilibrium entropy limiters have a great benefit: by summation of all entropy changes

we can estimate the amount of additional dissipation the limiters introduce into the system.

### C. Nondissipative recipes for stabilization

#### 1. Microscopic error and macroscopic accuracy

The invariant film  $\mathbf{q}$  is an invariant manifold for the free-flight transformation and for the temporal and entropic involutions. The linear involution  $I_0$ , as well as the ELBGK involution  $I_E$ , transforms a point  $f \in \mathbf{q}$  into a point  $f'$  with  $f - f' = \alpha \Delta_{\Pi^*(f)} + o(f - \Pi^*(f))$ , i.e., the vector  $f - f'$  is “almost tangent” to  $\mathbf{q}$ , and the distance from  $f'$  to  $\mathbf{q}$  has the order  $O(\|f - \Pi^*(f)\|^2)$ .

Hence, if the initial state belongs to  $\mathbf{q}$ , and the distance from quasiequilibrium is small enough [order  $O(h)$ ], then during several steps the LBGK chain will remain near  $\mathbf{q}$  with deviation of order  $O(h^2)$ . Moreover, because errors produced by collisions (deviations from  $\mathbf{q}$ ) have zero macroscopic projection, the corresponding macroscopic error in  $M$  during several steps will remain of order  $O(h^3)$ .

To demonstrate this, suppose the error in  $f$ ,  $\delta f$ , is of order  $O(h^k)$ , and  $m(\delta f) = 0$ , then for smooth fields after a free-flight step an error of higher order appears in the macroscopic variables  $M$ :  $m(\Theta_h(\delta f)) = O(h^{k+1})$ , because  $m(\Theta_h(\delta f)) = m((\Theta_h - 1)(\delta f))$  and  $\Theta_h - 1 = O(h)$ . The last estimate requires smoothness.

This simple statement is useful for the error analysis we perform. We shall call it the *lemma of higher macroscopic accuracy*: a microscopic error of order  $O(h^k)$  induces, after a time step  $h$ , a macroscopic error of order  $O(h^{k+1})$ , if the field of macroscopic fluxes is sufficiently small (here, the microscopic error means the error that has zero macroscopic projection).

#### 2. Restarts and approximation of $\Delta_{f_M^*}$

The problem of nondissipative LBM stabilization we interpret as a problem of appropriate restart from a point that is sufficiently close to the invariant film. If  $h = \tau$  and collisions return the state to quasiequilibrium, then the state belongs to  $\mathbf{q}$  for all time with high accuracy. For  $h \neq \tau$ , formulas for restarting are also available: one can choose between Eq. (22) and, more flexibly, Eq. (23). Nevertheless, many questions remain. First, what should one take for  $\Delta_{f_M^*}$ ? This vector has a straightforward differential definition (10) [let us also recall that  $\tau \Delta_{f_M^*}$  is the first Chapman-Enskog nonequilibrium correction to the distribution function (19)]. But numerical differentiation could violate the exact-in-space free-flight transformation and local collisions. There exists a rather accurate central difference approximation of  $\Delta_{f_M^*}$  on the basis of free flight:

$$\Delta_{f_M^*} = \frac{1}{2}(\Delta_{f_M^*}^+ + \Delta_{f_M^*}^-) + O(h^2), \quad (41)$$

where

$$\Delta_{f_M^*}^+ = \frac{1}{h}[\Theta_h(f_M^*) - \Pi^*(\Theta_h(f_M^*))],$$

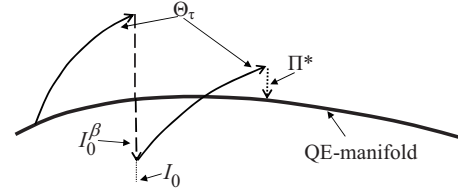


FIG. 4. The scheme of coupled steps (43).

$$\Delta_{f_M^*}^- = -\frac{1}{h}[\Theta_{-h}(f_M^*) - \Pi^*(\Theta_{-h}(f_M^*))].$$

There are no errors of the first order in Eq. (41). The forward ( $\Delta_{f_M^*}^+$ ) and backward ( $\Delta_{f_M^*}^-$ ) approximations are one order less accurate. The computation of  $\Delta_{f_M^*}^\pm$  is of the same computational cost as an LBGK step, hence, if we use the restart formula (22) with central difference evaluation of  $\Delta_{f_M^*}$  (41), then the computational cost increases three times (approximately). Nonlocality of collisions [restart from the distribution  $f_M^*$  (22) with a nonlocal expression for  $\Delta_{f_M^*}$ ] spoils the main LBM idea of exact linear free flight and local collisions: nonlocality is linear and exact, nonlinearity is local [1]. One might also consider the inclusion of other finite difference representations for  $\Delta_{f_M^*}$  into explicit LBM schemes. The consequences of this combination should be investigated.

#### 3. Coupled steps with quasiequilibrium ends

The mean viscosity lemma allows us to combine different starting points in order to obtain the necessary macroscopic equations. From this lemma, it follows that the following construction of two coupled steps with restart from quasiequilibrium approximates the macroscopic equation (9) with second-order accuracy in time step  $h$ .

Let us take  $f_M^*$  as the initial state with given  $M$ , then evolve the state by  $\Theta_h$ , apply the incomplete temporal involution  $I_T^\beta$  (28), again evolve by  $\Theta_h$ , and finally project by  $\Pi^*$  onto the quasiequilibrium manifold:

$$M \mapsto M' = m(\Pi^*(\Theta_h(I_T^\beta(\Theta_h(f_M^*))))). \quad (42)$$

It follows from the restart formula (22) and the mean viscosity lemma that this step gives a second order in time  $h$  approximation to the shift in time  $2h$  for Eq. (9) with  $\tau = 2(1 - \beta)h$ ,  $1/2 \leq \beta \leq 1$ . Now, let us replace  $I_T^\beta$  by the much simpler transformation of LBGK collisions  $I_0^\beta$  (33):

$$M \mapsto M' = m(\Pi^*(\Theta_h(I_0^\beta(\Theta_h(f_M^*))))). \quad (43)$$

According to the lemma of higher macroscopic accuracy this step (Fig. 4) also gives a second order in time  $h$  approximation to the shift in time  $2h$  for Eq. (9) with  $\tau = 2(1 - \beta)h$ ,  $1/2 \leq \beta \leq 1$ . The replacement of  $I_T^\beta$  by  $I_0^\beta$  introduces an error in  $f$  that is of order  $O(h^2)$ , but both transformations conserve the value of macroscopic variables exactly. Hence (due to the lemma of higher macroscopic accuracy) the resulting error of coupled steps (43) in the macroscopic variables  $M$  is of order  $O(h^3)$ . This means that the method has second-order accuracy.

Let us enumerate the macroscopic states in Eq. (43):  $M_0 = M$ ,  $M_{1/2} = m(\Theta_h(f_M^*))$ , and  $M_1 = M'$ . The shift from  $M_0$  to  $M_{1/2}$  approximates the shift in time  $h$  for Eq. (9) with  $\tau = h$ . If we would like to model (9) with  $\tau \ll h$ , then  $\tau = h$  means relatively very high viscosity. The step from  $M_{1/2}$  to  $M_1$  has to normalize viscosity to the requested small value (compare to *antidiffusion* in [39,40]). The antidiffusion problem necessarily appears in most CFD approaches to simulation flows with high-Reynolds numbers. Another famous example of such a problem is the filtering-defiltering problem in large eddy simulation (LES) [44]. The antidiffusion in the coupled steps is produced by physical fluxes (by free flight) and preserves positivity. The coupled step is a transformation  $M_0 \mapsto M_1$  and takes time  $2h$ . The middle point  $M_{1/2}$  is an auxiliary state only.

Let us enumerate the microscopic states in Eq. (43):  $f_0 = f_M^*$ ,  $f_{1/2}^- = \Theta_h(f_M^*)$ ,  $f_{1/2}^0 = \Pi^*(f_{1/2}^-)$ ,  $\tilde{f}_{1/2} = I_0^1(f_{1/2}^-)$ ,  $f_{1/2}^+ = f_{1/2}^0 + (1-\beta)(\tilde{f}_{1/2} - f_{1/2}^0)$ ,  $f_1 = \Theta_h(f_{1/2}^+)f_1 = \Pi^*(f_1^+) = f_{M_1}^*$ , where  $M_1 = m(f_1^+)$ . Here, in the middle of the step, we have four points: a free-flight shift of the initial state ( $f_{1/2}^-$ ), the corresponding quasiequilibrium ( $f_{1/2}^0$ ), the mirror image ( $\tilde{f}_{1/2}$ ) of the point  $f_{1/2}^-$  with respect to the center  $f_{1/2}^0$ , and the state ( $f_{1/2}^+$ ) that is the image of  $f_{1/2}^-$  after homothety with center  $f_{1/2}^0$  and coefficient  $2\beta - 1$ .

For smooth fields, the time shift  $\Theta_h$  returns  $\tilde{f}_{1/2}$  to the quasiequilibrium manifold with possible error of order  $O(h^2)$ . For entropic equilibria, the nonequilibrium entropy of the state  $\Theta_h(\tilde{f}_{1/2})$  is of order  $O(h^4)$ . This is an entropic estimate of the accuracy of antidiffusion: the nonequilibrium entropy of  $\tilde{f}_{1/2}$  could be estimated from below as  $C(M)h^2$ , where  $C(M) > 0$  does not depend on  $h$ . The problem of antidiffusion can be stated as an implicit stepping problem: find a point  $\tilde{f}$  such that

$$m(\tilde{f}) = M, \quad (\Pi^* - 1)(\Theta_h(\tilde{f})) = 0. \quad (44)$$

This *antidiffusion problem* is a proper two-point boundary value problem. In a finite-dimensional space the first condition includes  $N$  independent equations (where  $N$  is the number of independent macroscopic variables), the second allows  $N$  degrees of freedom, because the values of the macroscopic variables at that end are not fixed and  $\Theta_h(\tilde{f})$  could be any point on the quasiequilibrium manifold. Shooting methods for the solution of this problem looks quite simple: (a) method A,

$$\tilde{f}_{n+1} = \tilde{f}_n + \Pi^*(\Theta_h(\tilde{f}_n)) - \Theta_h(\tilde{f}_n), \quad (45)$$

(b) method B,

$$\tilde{f}_{n+1} = \Theta_{-h}(\Pi^*(\Theta_h(\tilde{f}_n))) + f_M^* - \Pi^*(\Theta_{-h}(\Pi^*(\Theta_h(\tilde{f}_n)))). \quad (46)$$

Method A is shoot from the previous approximation,  $\tilde{f}_n$ , by  $\Theta_h$ , project onto quasiequilibrium,  $\Pi^*(\Theta_h(\tilde{f}_n))$ , and then correction of  $\tilde{f}_n$  by the final point displacement,  $\Pi^*(\Theta_h(\tilde{f}_n))$

$-\Theta_h(\tilde{f}_n)$ . The value of  $M$  does not change, because  $m(\Pi^*(\Theta_h(\tilde{f}_n))) = m(\Theta_h(\tilde{f}_n))$ .

Method B is shoot from the previous approximation,  $\tilde{f}_n$ , by  $\Theta_h$ , project onto quasiequilibrium, shoot backwards by  $\Theta_{-h}$ , and then correction of  $M$  using quasiequilibria (plus the quasiequilibrium with required value of  $M$ , and minus one with current value of  $M$ ).

The initial approximation could be  $\tilde{f}_{1/2}$ , and  $n$  here is the number of iteration. Due to the lemma of higher macroscopic accuracy, each iteration (45) or (46) increases the order of accuracy (see also the numerical test in Sec. IV).

The shooting method A (45) better meets the main LBM idea: each change of macroscopic variable is due to a free flight step (because free flight in LBM is exact), all other operations effect nonequilibrium component of the distribution only. The correction of  $M$  in the shooting method B (46) violates this requirement.

The idea that all macroscopic changes are projections of free flight plays, for the proposed LBM antidiffusion, the same role as the monotonicity condition for FCT [39]. In particular, free flight never violates positivity.

If we find solution  $\tilde{f}$  to the antidiffusion problem with  $M = M_{1/2}$ , then we can take  $f_{1/2}^+ = f_{1/2}^0 + (1-\beta)(\tilde{f} - f_{1/2}^0)$ , and  $M_1 = m(\Theta_h(f_{1/2}^+))$ . But even exact solutions of Eq. (44) can cause stability problems: the entropy of  $\tilde{f}$  could be less than the entropy of  $f_{1/2}^-$ , and blowup could appear. A palliative solution is to perform an entropic step: to find  $\alpha$  such that  $S(f_{1/2}^0 + \alpha(\tilde{f} - f_{1/2}^0)) = S(f_{1/2}^-)$ , then use  $f_{1/2}^+ = f_{1/2}^0 + (1-\beta)\alpha(\tilde{f} - f_{1/2}^0)$ . Even for nonentropic equilibria it is possible to use the Kullback entropy (39) for comparison of distributions with the same value of the macroscopic variables. Moreover, the quadratic approximation to Eq. (39) will not violate second-order accuracy, and does not require the solution of a transcendental equation.

The viscosity coefficient is proportional to  $\tau$  and significantly depends on the chain construction: for the sequence (29) we have  $\tau = (1-\beta)h/\beta$ , and for the sequence of steps (43)  $\tau = 2(1-\beta)h$ . For small  $1-\beta$  the later gives around two times larger viscosity (and for realization of the same viscosity we must take this into account).

How can the coupled steps method (43) fail? The method collects all the high-order errors into dissipation. When the high-order errors accumulated in dissipation become compatible with the second-order terms, the observable viscosity significantly increases. In our numerical tests this catastrophe occurs when the hydrodynamic fields change significantly on 2–3 grid steps  $\delta_x$  (the characteristic wavelength  $\lambda \approx 3\delta_x$ ). The catastrophe point is the same for the plain coupled steps (43) and for the methods with iterative corrections (45) or (46). The appropriate accuracy requires  $\lambda \gtrsim 10\delta_x$ . On the other hand, this method is a good solver for problems with shocks (in comparison with standard LBGK and ELBGK) and produces shock waves with very narrow fronts and almost without Gibbs effect. So, for sufficiently smooth fields it should demonstrate second-order accuracy, and in the vicinity of steep velocity derivatives it increases viscosity and produces artificial dissipation. Hence, this recipe is nondissipative in the main order only.

The main technical task in “stabilization for accuracy” is to keep the system sufficiently close to the invariant film. Roughly speaking, we should correct the microscopic state  $f$  in order to keep it close to the invariant film or to the tangent straight line  $\{f_M^* + \lambda \Delta_{f_M^*} | \lambda \in \mathbb{R}\}$ , where  $M = m(f)$ . But the general accuracy condition (23) gives much more freedom: the restart point should return to the invariant film in projections on the macroscopic variables and their fluxes only. A variant of such regularization was *de facto* proposed and successfully tested in [45]. In the simplest realization of such approaches a problem of “ghost” variables [1] can arise: when we change the restart (22) and (23), neither moments, nor fluxes change. The difference is a “ghost” vector. At the next step, the introduced ghost component could affect fluxes, and at the following steps the coupling between ghost variables and macroscopic moments emerges. Additional relaxation times may be adjusted to suppress these nonhydrodynamic ghost variables [46].

#### 4. Compromise between nonequilibrium memory and restart rules

Formulas (22) and (23) prescribe a choice of restart states  $f_M^s$ . All memory from previous evolution is in the macroscopic state,  $M$ , only. There is no microscopic (or, alternatively, nonequilibrium) memory. Effects of nonequilibrium memory for LBM are not yet well studied. For LBGK with overrelaxation, these effects increase when  $\beta$  approaches 1 because relaxation time increases.

One can formulate a hypothesis: observed subgrid properties of various LBGK realization and modifications for high-Reynolds number are due to nonequilibrium memory effects. The necessity of nonequilibrium memory for turbulence modeling is still an open question.

In order to find a compromise between the restart requirements (22) and (23) and nonequilibrium memory existence one can choose directions in concordance with (22) and (23), where the nonequilibrium entropy field (38) does not change in the restart procedure. If after a free-flight step we have a distribution  $f$  and find a corresponding restart state  $f_{m(f)}^s$  due to a global rule, then for each grid point  $\mathbf{x}$  we can restart from a point  $f_{m(f)}^* + \alpha(\mathbf{x})(f_{m(f)}^s - f_{m(f)}^*)$ , where  $\alpha(\mathbf{x}) > 0$  is a solution of the constant local nonequilibrium entropy equation  $S(f_{m(f)}^*(\mathbf{x}) + \alpha(\mathbf{x})[f_{m(f)}^s(\mathbf{x}) - f_{m(f)}^*(\mathbf{x})]) = S(f(\mathbf{x}))$ . This family of methods allows a minimal nonequilibrium memory—the memory about local entropic distance from quasiequilibrium.

## IV. NUMERICAL EXPERIMENT

### A. Velocities and equilibria

To conclude this paper we report numerical experiments conducted to demonstrate the performance of some of the proposed LBM stabilization recipes from Sec. III.

We choose velocity sets with entropic equilibria and an  $H$  theorem in order to compare all methods in a uniform setting.

In 1D, we use a lattice with spacing and time step  $h=1$  and a discrete velocity set  $\{v_1, v_2, v_3\} := \{0, -1, 1\}$  so that the model consists of static, left- and right-moving populations

only. The subscript  $i$  denotes population (not lattice site number) and  $f_1$ ,  $f_2$ , and  $f_3$  denote the static, left-, and right-moving populations, respectively. The entropy is  $S = -H$ , with

$$H = f_1 \ln(f_1/4) + f_2 \ln(f_2) + f_3 \ln(f_3)$$

(see, e.g., [47]) and, for this entropy, the local quasiequilibrium state  $f^*$  is available explicitly:

$$f_1^* = \frac{2n}{3}(2 - \sqrt{1 + 3u^2}),$$

$$f_2^* = \frac{n}{6}[(3u - 1) + 2\sqrt{1 + 3u^2}],$$

$$f_3^* = -\frac{n}{6}[(3u + 1) - 2\sqrt{1 + 3u^2}],$$

where

$$n := \sum_i f_i, \quad u := \frac{1}{n} \sum_i v_i f_i.$$

In 2D, the realization of LBGK that we use will employ a uniform nine-speed square lattice with discrete velocities  $\{v_i | i=0, 1, \dots, 8\}$ :  $v_0=0$ ,  $v_i = [\cos((i-1)\pi/2), \sin((i-1)\pi/2)]$  for  $i=1, 2, 3, 4$ ,  $v_i = \sqrt{2}[\cos[(i-5)\frac{\pi}{2} + \frac{\pi}{4}], \sin[(i-5)\frac{\pi}{2} + \frac{\pi}{4}]]$  for  $i=5, 6, 7, 8$ . The numbering  $f_0, f_1, \dots, f_8$  are for the static, east, north, west, south, northeast, northwest, southwest, and southeast moving populations, respectively. As usual, the quasiequilibrium state,  $f^*$ , can be uniquely determined by maximizing an entropy functional

$$S(f) = - \sum_i f_i \ln\left(\frac{f_i}{W_i}\right),$$

subject to the constraints of conservation of mass and momentum [48]:

$$f_i^* = n W_i \prod_{j=1}^2 (2 - \sqrt{1 + 3u_j^2}) \left( \frac{2u_j + \sqrt{1 + 3u_j^2}}{1 - u_j} \right)^{v_{i,j}}. \quad (47)$$

Here, the *lattice weights*,  $W_i$ , are given lattice-specific constants:  $W_0=4/9$ ,  $W_{1,2,3,4}=1/9$  and  $W_{5,6,7,8}=1/36$ . The macroscopic variables are given by the expressions

$$n := \sum_i f_i, \quad (u_1, u_2) := \frac{1}{n} \sum_i v_i f_i.$$

As we are advised in Sec. III, in all of the experiments, we implement the positivity rule.

### B. Shock tube

The 1D shock tube for a compressible isothermal fluid is a standard benchmark test for hydrodynamic codes. Our computational domain will be the interval  $[0, 1]$  and we discretize this interval with 801 uniformly spaced lattice sites. We choose the initial density ratio as 1:2 so that for  $x \leq 400$  we set  $n=1.0$ , else we set  $n=0.5$ .

**1. Basic test: lattice Bhatnager-Gross-Krook method,  
entropic lattice Bhatnager-Gross-Krook method  
and coupled steps**

We will fix the kinematic viscosity of the fluid at  $\nu = 10^{-9}$ . We should take  $\beta = 1/(2\nu + 1) \approx 1 - 2\nu$  for LBGK and ELBGK (with or without the Ehrenfests' regularization). Whereas, for the coupled step regularization, we should take  $\beta = 1 - \nu$ .

The governing equations for LBGK are

$$f_i(x + v_i, t + 1) = f_i^*(x, t) + (2\beta - 1)[f_i^*(x, t) - f_i(x, t)]. \quad (48)$$

For ELBGK (35) the governing equations are

$$f_i(x + v_i, t + 1) = (1 - \beta)f_i^*(x, t) + \beta\tilde{f}_i(x, t), \quad (49)$$

with  $\tilde{f} = (1 - \alpha)f + \alpha f^*$ . As previously mentioned, the parameter,  $\alpha$ , is chosen to satisfy a constant entropy condition. This involves finding the nontrivial root of the equation

$$S[(1 - \alpha)f + \alpha f^*] = S(f). \quad (50)$$

Inaccuracy in the solution of this equation can introduce artificial viscosity. To solve Eq. (50) numerically we employ a robust routine based on bisection. The root is solved to an accuracy of  $10^{-15}$  and we always ensure that the returned value of  $\alpha$  does not lead to a numerical entropy decrease. We stipulate that if, at some site, no nontrivial root of Eq. (50) exists we will employ the positivity rule instead.

The governing equations for the coupled step regularization of LBGK alternates between classic LBGK steps and equilibration:

$$f_i(x + v_i, t + 1) = \begin{cases} f_i^*(x, t), & N_{\text{step}} \text{ odd} \\ f_i^*(x, t) + (2\beta - 1)[f_i^*(x, t) - f_i(x, t)], & N_{\text{step}} \text{ even,} \end{cases} \quad (51)$$

where  $N_{\text{step}}$  is the cumulative total number of time steps taken in the simulation. For coupled steps, only the result of a couple of steps has clear physical meaning: this couple transforms  $f_i^*(x, t)$  that appears at the beginning of an odd step to  $f_i^*(x, t)$  that appears at the beginning of the next odd step.

As we can see, the choice between the two collision formulas LBGK (48) or ELBGK (49) does not affect spurious oscillation (see Fig. 5). But it should be mentioned that the entropic method consists of not only the collision formula, but, what is important, includes the provision of special choices of quasiequilibrium that could improve stability (see, e.g., [24]). The coupled steps produce almost no spurious oscillations. This seems to be good, but in such cases it is necessary to monitor the amount of artificial dissipation and to measure the viscosity provided by the method (see below).

**2. Ehrenfests' regularization**

For the realization of the Ehrenfests' regularization of LBGK, which is intended to keep states uniformly close to

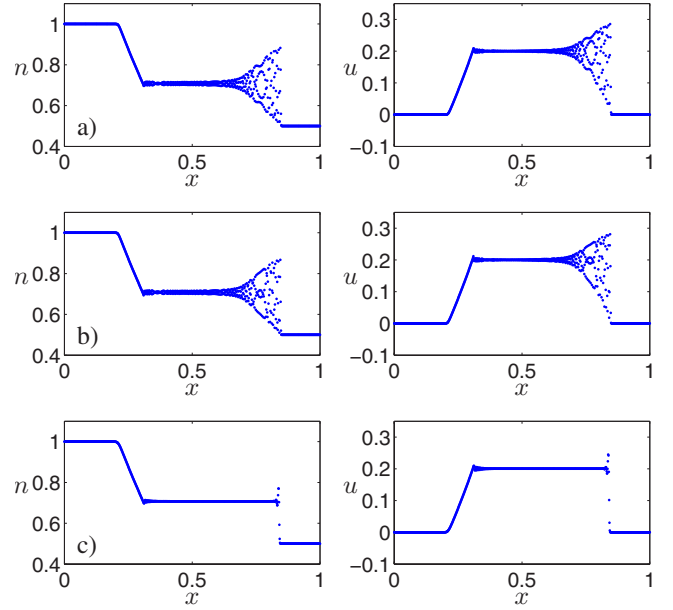


FIG. 5. (Color online) Density and velocity profile of the 1:2 isothermal shock tube simulation after 400 time steps using (a) LBGK (48); (b) ELBGK (49); (c) coupled step regularization (51); In this example, no negative population are produced by any of the methods so the positivity rule is redundant. For ELBGK in this example, Eq. (50) always has a nontrivial root.

the quasiequilibrium manifold, we should monitor nonequilibrium entropy  $\Delta S$  (38) at every lattice site throughout the simulation. If a prespecified threshold value  $\delta$  is exceeded, then an Ehrenfests' step is taken at the corresponding site. Now, the governing equations become

$$f_i(x + v_i, t + 1) = \begin{cases} f_i^*(x, t) + (2\beta - 1)[f_i^*(x, t) - f_i(x, t)], & \Delta S \leq \delta \\ f_i^*(x, t), & \text{otherwise,} \end{cases} \quad (52)$$

Furthermore, so that the Ehrenfests' steps are not allowed to degrade the accuracy of LBGK it is pertinent to select the  $k$  sites with highest  $\Delta S > \delta$ . The *a posteriori* estimates of added dissipation could easily be performed by analysis of entropy production in Ehrenfests' steps.

In the example in Fig. 6, we have considered fixed tolerances of  $(k, \delta) = (4, 10^{-3})$  and  $(k, \delta) = (4, 10^{-4})$  only. We reiterate that it is important for Ehrenfests' steps to be employed at only a small share of sites. To illustrate, in Fig. 7 we have allowed  $k$  to be unbounded and let  $\delta$  vary. As  $\delta$  decreases, the number of Ehrenfests' steps quickly begins to grow (as shown in the accompanying histograms) and excessive and unnecessary smoothing is observed at the shock. The second-order accuracy of LBGK is corrupted. In Fig. 8, we have kept  $\delta$  fixed at  $\delta = 10^{-4}$  and instead let  $k$  vary. We observe that even small values of  $k$  (e.g.,  $k = 1$ ) dramatically improves the stability of LBGK.

**C. Accuracy of coupled steps**

Coupled steps (43) give the simplest second-order accurate stabilization of LBGK. Stabilization is guaranteed by

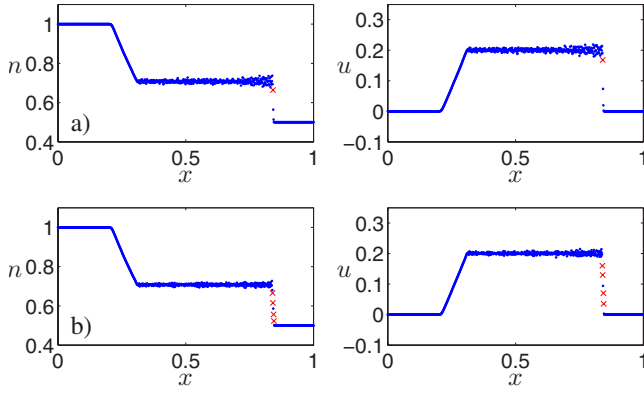


FIG. 6. (Color online) Density and velocity profile of the 1:2 isothermal shock tube simulation after 400 time steps using Ehrenfest's regularization (52) with (a)  $(k, \delta) = (4, 10^{-3})$ ; (b)  $(k, \delta) = (4, 10^{-4})$ . Sites where Ehrenfest's steps are employed are indicated by crosses. Compare to Fig. 5(a).

collection of all errors into dissipative terms. But this monotone collection of errors could increase the higher-order terms in viscosity. Hence, it seems to be necessary to analyze not only order of errors, but their values, too.

For accuracy analysis of coupled steps we are interested in the error in the antidiffusion step (44). We analyze one coupled step for  $\beta=1$ . The motion starts from a quasiequilibrium  $f_0 = f_M^*$ , then a free-flight step  $f_{1/2}^- = \Theta_h(f_M^*)$ , after that a simple reflection  $\tilde{f}_{1/2} = I_0^1(f_{1/2}^-)$  with respect to the quasiequilibrium center  $f_{1/2}^0 = \Pi^*(f_{1/2}^-)$ , again a free-flight step,  $f_1^- = \Theta_h(\tilde{f}_{1/2})$ , and finally a projection onto quasiequilibrium,  $f_1 = \Pi^*(f_1^-)$ .

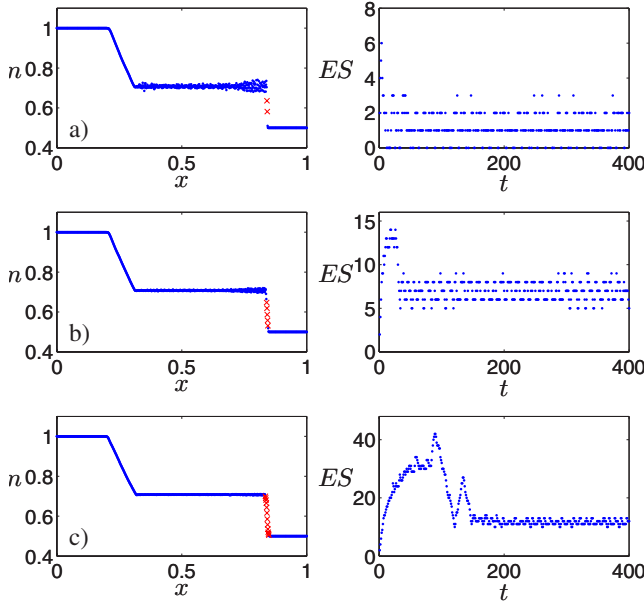


FIG. 7. (Color online) LBGK (48) regularized with Ehrenfest's steps (52). Density profile of the 1:2 isothermal shock tube simulation and Ehrenfest's steps histogram after 400 time steps using the tolerances (a)  $(k, \delta) = (\infty, 10^{-3})$ ; (b)  $(k, \delta) = (\infty, 10^{-4})$ ; (c)  $(k, \delta) = (\infty, 10^{-5})$ . Sites where Ehrenfest's steps are employed are indicated by crosses. Compare to Fig. 5(a).

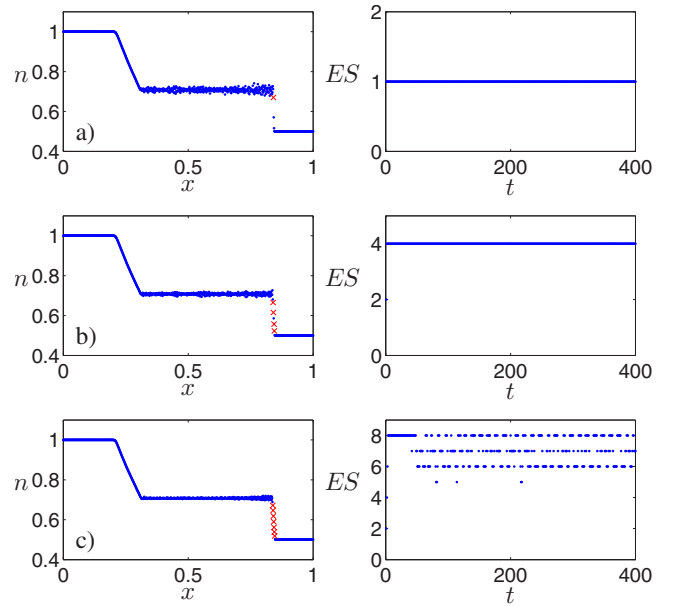


FIG. 8. (Color online) LBGK (48) realization with Ehrenfest's steps (52). Density profile of the 1:2 isothermal shock tube simulation and Ehrenfest's steps histogram after 400 time steps using the tolerances (a)  $(k, \delta) = (1, 10^{-4})$ ; (b)  $(k, \delta) = (4, 10^{-4})$ ; (c)  $(k, \delta) = (8, 10^{-4})$ . Sites where Ehrenfest's steps are employed are indicated by crosses. Compare to Fig. 5(a).

In the first of two accuracy tests, two types of errors are to be studied. The middle point displacement is

$$\delta_{cs} = \|f_{1/2}^0 - \Pi^*(\Theta_{-h}(f_1^-))\| / \|f_0 - f_{1/2}^0\|. \quad (53)$$

To estimate nonequilibrium of the final point  $f_1^-$  (i.e., additional dissipation introduced by last projection in the coupled step) we should compare the difference  $f_1^- - f_1$  to the difference at the middle point  $f_{1/2}^- - f_{1/2}^0$ . Let us introduce

$$\sigma_{cs} = \|f_1^- - f_1\|^2 / \|f_{1/2}^- - f_{1/2}^0\|^2. \quad (54)$$

In our tests (Fig. 9) we use the  $\ell_2$  norm.

We take the 1D three-velocity model with entropic equilibria. Our computational domain will be the interval  $[0, 1]$  which we discretize with 1001 uniformly spaced lattice sites. The initial condition is  $n(x, 0) = 1 + 0.2 \sin(2\pi\omega x)$ ,  $u(x, 0) = 0.1 \cos(2\pi\omega x)$  and we employ periodic boundary conditions. We compute a single coupled step for frequencies in the range  $\omega = 1, 2, \dots, 1000$  (Fig. 9).

The solution  $\tilde{f}$  to the antidiffusion problem could be corrected by the shooting iterations (45) and (46). The corresponding errors for method B (46) are also presented in Fig. 9. We use  $\delta_{cs,i}$  and  $\sigma_{cs,i}$  for  $i=1, 2, \dots$ , to denote each subsequent shooting of Eqs. (53) and (54), respectively.

We observe that the nonequilibrium estimate,  $\sigma_{cs}$ , blows up around the wavelength  $1/\omega \approx 3\delta_x$ . Simultaneously, the middle point displacement  $\delta_{cs}$  has value around unity at the same point. We do not plot the results for larger values of  $\omega$  as the simulation has become meaningless and numerical aliasing will now decrease these errors. The same critical

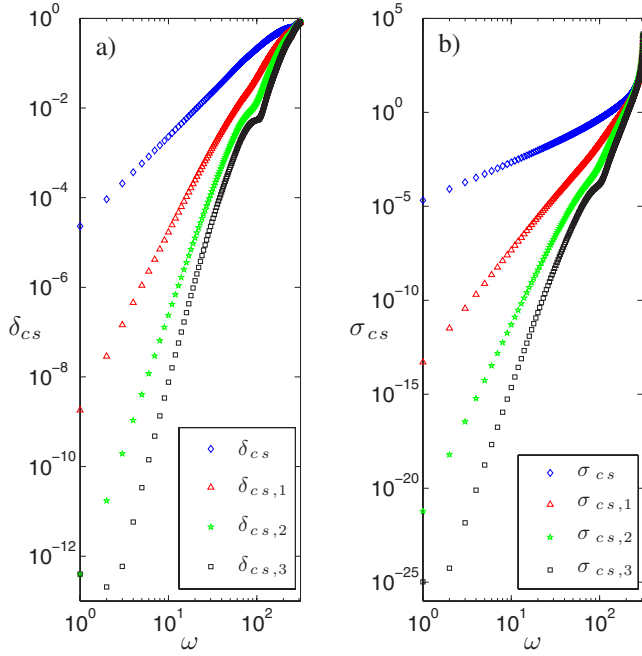


FIG. 9. (Color online) (a) The  $\ell_2$  estimate of middle point displacement (53): for coupled steps (43) (diamonds), one (triangles), two (squares), and three (dots) shooting iterations (46); (b) The  $\ell_2$  estimate of nonequilibrium of the final point (54): for coupled steps (43) (diamonds), one (triangles), two (stars), and three (squares) shooting iterations (46).

point is observed for each subsequent shooting as well. For this problem, the shooting procedure is demonstrated to be effective for wavenumbers  $1/\omega \leq 10\delta_x$ .

For the second accuracy test we propose a simple test to measure the observable viscosity of a coupled step (and LBGK) simulation. We take the 2D isothermal nine-velocity model with entropic equilibria. Our computational domain will be a square which we discretize with  $(L+1) \times (L+1)$  uniformly spaced points and periodic boundary conditions. The initial condition is  $n(x,y)=1$ ,  $u_1(x,y)=0$ , and  $u_2(x,y)=u_0 \sin(2\pi x/L)$ , with  $u_0=0.05$ . The exact velocity solution to this problem is an exponential decay of the initial condition:  $u_1(x,y,t)=0$ ,  $u_2(x,y,t)=u_0 \exp(-\lambda u_0 t / (\text{Re} L)) \sin(2\pi x/L)$ , where  $\lambda$  is some constant and  $\text{Re}=\text{Re}(\beta)=u_0 L / \nu(\beta)$  is the Reynolds number of the flow. Here,  $\nu=\nu(\beta)$  is the theoretical viscosity of the fluid:  $\nu=1-\beta$  for the coupled steps (43) and  $\nu=(1/\beta-1)/2$  for LBGK.

Now, we simulate the flow over  $L/\nu_0$  time steps and measure the constant  $\lambda$  from the numerical solution. We do this for both LBGK and the coupled steps (43) for  $L=100$  and for  $L=200$ . The results (Fig. 10) show us that for coupled steps (and for LBGK to a much lesser extent) the observed viscosity is higher than the theoretical estimate, hence the observed  $\text{Re}$  is lower than the estimate. In particular, the lower-resolution ( $L=100$ ) coupled steps simulation diverges from LBGK at around  $\text{Re}=500$ . The two times higher-resolution ( $L=200$ ) simulations are close to around  $\text{Re} \sim 1000$ , after which there begins to be a considerable increase in the observable viscosity (as explained within Sec. III C).

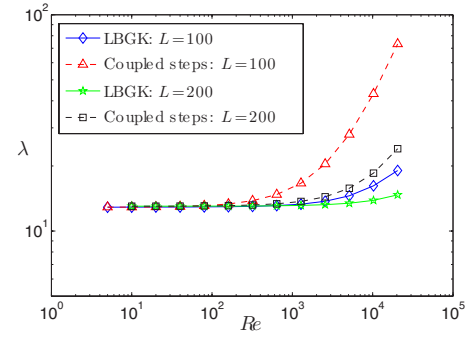


FIG. 10. (Color online) Numerically computed value of  $\lambda$  versus Reynolds number for 2D accuracy test: LBGK with  $L=100$  (diamonds); coupled steps (43) with  $L=100$  (triangles); LBGK with  $L=200$  (stars); coupled steps (43) with  $L=200$  (squares).

#### D. Flow around a square cylinder

The unsteady flow around a square cylinder has been widely experimentally investigated in the literature (see, e.g., [49–51]). The computational setup for the flow is as follows. A square cylinder of side length  $L$ , initially at rest, is immersed in a constant flow in a rectangular channel of length  $30L$  and height  $25L$ . The cylinder is placed on the center line in the  $y$  direction resulting in a blockage ratio of 4%. The center of the cylinder is placed at a distance  $10.5L$  from the inlet. The free-stream velocity is fixed at  $(u_\infty, v_\infty)=(0.05, 0)$  (in lattice units) for all simulations.

On the north and south channel walls a free-slip boundary condition is imposed (see, e.g., [1]). At the inlet, the inward pointing velocities are replaced with their quasiequilibrium values corresponding to the free-stream velocity. At the outlet, the inward pointing velocities are replaced with their associated quasiequilibrium values corresponding to the velocity and density of the penultimate row of the lattice.

##### 1. Maxwell boundary condition

The boundary condition on the cylinder that we prefer is the diffusive Maxwell boundary condition (see, e.g., [52]), which was first applied to LBM in [53]. The essence of the condition is that populations reaching a boundary are reflected, proportional to equilibrium, such that mass balance (in the bulk) and detail balance are achieved. We will describe two possible optimizations of the boundary condition—time delayed and instantaneous reflection of equilibrated populations. In both instances, immediately prior to the advection of populations, only those populations pointing in to the fluid at a boundary site are updated. Boundary sites do not undergo the collisional step that the bulk of the sites are subjected to.

To illustrate, consider the situation of a wall, aligned with the lattice, moving with velocity  $u_{\text{wall}}$  and with outward pointing normal to the wall pointing in the positive  $y$  direction (this is the situation on the north wall of the square cylinder with  $u_{\text{wall}}=0$ ). The time-delayed reflection implementation of the diffusive Maxwell boundary condition at a boundary site  $(x,y)$  on this wall consists of the update

$$f_i(x,y,t+1) = \alpha f_i^*(u_{\text{wall}}), \quad i = 2, 5, 6,$$

with

$$\alpha = \frac{f_4(x, y, t) + f_7(x, y, t) + f_8(x, y, t)}{f_2^*(u_{\text{wall}}) + f_5^*(u_{\text{wall}}) + f_6^*(u_{\text{wall}})}.$$

Whereas for the instantaneous reflection implementation we should use for  $\alpha$ ,

$$\frac{f_4(x, y + 1, t) + f_7(x + 1, y + 1, t) + f_8(x - 1, y + 1, t)}{f_2^*(u_{\text{wall}}) + f_5^*(u_{\text{wall}}) + f_6^*(u_{\text{wall}})}.$$

Observe that, because density is a linear factor of the equilibria (47), the density of the wall is inconsequential in the boundary condition and can therefore be taken as unity for convenience.

We point out that, although both optimization agree in the continuum limit, the time-delayed implementation does not accomplish mass balance. Therefore, instantaneous reflection is preferred and will be the implementation that we employ in the present example.

Finally, it is instructive to illustrate the situation for a boundary site  $(x, y)$  on a corner of the square cylinder, say the northwest corner. The (instantaneous reflection) update is then

$$f_i(x, y, t + 1) = \beta f_i^*(u_{\text{wall}}), \quad i = 2, 3, 5, 6, 7,$$

where

$$\beta = \beta_0 / \beta_{\text{wall}};$$

$$\beta_0 = f_1(x - 1, y, t) + f_4(x, y + 1, t) + f_5(x - 1, y - 1, t) + f_7(x + 1, y + 1, t) + f_8(x - 1, y + 1, t);$$

$$\beta_{\text{wall}} = f_2^*(u_{\text{wall}}) + f_3^*(u_{\text{wall}}) + f_5^*(u_{\text{wall}}) + f_6^*(u_{\text{wall}}) + f_7^*(u_{\text{wall}}).$$

## 2. Strouhal-Reynolds relationship

As a test of the Ehrenfests' regularization (52), a series of simulations, all with characteristic length fixed at  $L=20$ , were conducted over a range of Reynolds numbers  $Re = Lu_{\infty} / \nu$ . The parameter pair  $(k, \delta)$ , which control the Ehrenfests' steps tolerances, are fixed at  $(L/2, 10^{-3})$ .

We are interested in computing the Strouhal-Reynolds relationship. The Strouhal number  $St$  is a dimensionless measure of the vortex shedding frequency in the wake of one side of the cylinder:  $St = Lf_{\omega} / u_{\infty}$ , where  $f_{\omega}$  is the shedding frequency.

For our computational set up, the vortex shedding frequency is computed using the following algorithmic technique. First, the  $x$  component of velocity is recorded during the simulation over  $t_{\text{max}} = 1250L / u_{\infty}$  time steps. The monitoring points is positioned at coordinates  $(4L, -2L)$  (assuming the origin is at the center of the cylinder). Next, the dominant frequency is extracted from the final 25% of the signal using the discrete Fourier transform. The monitoring point is purposefully placed sufficiently downstream and away from the center line so that only the influence of one side of the cylinder is recorded.

The computed Strouhal-Reynolds relationship using the Ehrenfests' regularization of LBGK is shown in Fig. 11. The simulation compares well with Okajima's data from wind

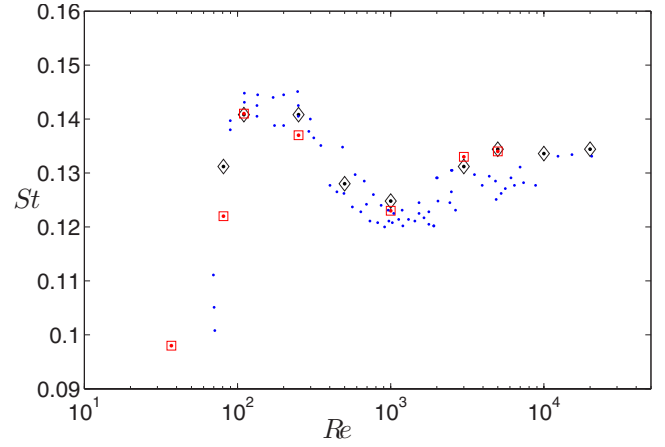


FIG. 11. (Color online) Variation of Strouhal number  $St$  as a function of Reynolds. Dots are Okajima's experimental data [51] (the data has been digitally extracted from the original paper). Diamonds are the Ehrenfests' regularization of LBGK and the squares are the ELBGK simulation from [19].

tunnel and water tank experiment [51]. The present simulation extends previous LBM studies of this problem [19,20] which have been able to quantitatively captured the relationship up to  $Re \sim 5000$ . Figure 11 also shows the ELBGK simulation results from [19]. Furthermore, the computational domain was fixed for all the present computations, with the smallest value of the kinematic viscosity attained being  $\nu = 5 \times 10^{-5}$  at  $Re = 20\,000$ . It is worth mentioning that, for this characteristic length, LBGK exhibits numerical divergence at around  $Re \sim 1000$ . We estimate that, for the present set up, the computational domain would require at least  $\sim 10^7$  lattice sites for the kinematic viscosity to be large enough for LBGK to converge at  $Re = 20\,000$ . This is compared with  $\sim 10^5$  sites for the present simulation.

## V. CONCLUSIONS

In this paper, we have analyzed LBM as a discrete dynamical system generated in distribution space by free flight for time  $\delta_t = h$  and involution (temporal or entropic, or just a standard LBGK reflection that approximates these involutions with second-order accuracy). Dissipation is produced by superposition of this involution with a homothety with center in quasiequilibrium and coefficient  $2\beta - 1$ .

Trajectories of this discrete dynamical system are projected onto the space of macroscopic variables, hydrodynamic fields, for example. The projection of a time step of the LBM dynamics in distribution space approximates a time shift for a macroscopic transport equation. We represent the general form of this equation (9), and provide necessary and sufficient conditions for this approximation to be of second-order accuracy in the time step  $h$  (22) and (23). This analysis includes conditions on the free-flight initial state, and does not depend on the particular collision model.

It is necessary to stress that for free flight the space discretization is exact (introduces no errors), if translation of the grid by vector  $\mathbf{v}_i \delta_t$  is the same grid for all velocities  $\mathbf{v}_i$ .

It seems natural to discuss the LBM discrete dynamical system as an approximate solution to the kinetic equation, for example, to the BGK kinetics with a discrete velocity set (1). With this kinetic equation we introduce one more time scale,  $\tau$ . For  $h \geq \tau$  (and overrelaxation) the discrete LBM does not give a second-order in time step  $h$  approximation to the continuous-in-time equation (1). This is obvious by comparison of “fast” direction relaxation times: it is  $\tau$  for Eq. (1) and  $h/[2(1-\beta)] \approx h^2/\tau$  for discrete dynamics (see also [10]). Nevertheless, the “macroscopic shadow” of the discrete LBM with overrelaxation approximates the macroscopic transport equation with second order in time step  $h$  accuracy under the conditions (22) and (23).

We have presented the some mechanisms of observed LBM instabilities: (1) positivity loss due to high local deviation from quasiequilibrium; (2) appearance of neutral stability in some directions in the zero viscosity limit; (3) directional instability. We have found three methods of stability preservation. Two of them, the positivity rule and the Ehrenfests’ regularization, are “salvation” (or “SOS”) operations. They preserve the system from positivity loss or from the local blowups, but introduce artificial dissipation and it is necessary to control the number of sites where these steps are applied. In order to preserve the second order of LBM accuracy, in average, at least, it is worthwhile to perform these steps on only a small number of sites; the number of sites should not be higher than  $O(N\delta_x/L)$ , where  $N$  is the total number of sites,  $L$  is the macroscopic characteristic length, and  $\delta_x$  is the lattice step. Moreover, because these steps have a tendency to concentrate in the most nonequilibrium regions (boundary layers, shock layers, etc.), instead of the total number of sites one can use an estimate of the number of sites in this region.

The positivity rule and the Ehrenfests’ regularization are members of a wide family of “nonequilibrium entropy limiters” that will play the same role, for LBM, as the flux limiters play for finite difference, finite volume, and finite element methods. We have described this family and explained how to use entropy estimates for nonentropic equilibria. The great benefit of the LBM methods is that the dissipation added by limiters could easily be estimated *a posteriori* by summarizing the entropy production.

Some practical recommendation for use of nonequilibrium entropy limiters are as follows:

(i) There exists a huge freedom in the construction of these limiters.

(ii) For any important class of problems a specific optimal limiter could be found.

(iii) One of the simplest and computationally cheapest nonequilibrium entropy limiters is the Ehrenfests’ regularization with equilibration at  $k$  sites with highest nonequilibrium entropy  $\Delta S > \delta$  [the  $(k, \delta)$  rule].

(iv) The positivity rule should always be implemented.

The developed restart methods (Sec. III C) (including coupled steps with quasiequilibrium ends) could provide

second-order accuracy, but destroy the memory of LBM. This memory emerges in LBM with overrelaxation because of slow relaxation of nonequilibrium degrees of freedom (there is no such memory in the continuous-in-time kinetic equation with fast relaxation to the invariant slow Chapman-Enskog manifold). Now, we have no theory of this memory but one can suggest a hypothesis that this memory is responsible for some of the LBM subgrid properties. A compromise between memory and stability is proposed: one can use the directions of restart to precondition collisions, and keep the memory in the value of the field of local nonequilibrium entropy  $\Delta S$  [or, for systems with nonentropic equilibria, in the value of the corresponding Kullback entropies (39)]. Formally, this preconditioning generates a matrix collision model [1] with a specific choice of matrix: in these models, the collision matrix is a superposition of projection (preconditioner), involution, and homothety. A return from the simplest LBGK collision to matrix models has been intensively discussed recently in development of the multirelaxation time (MRT) models (for example, [54,55], see also [56] for matrix models for localized of nonisotropic advection-diffusion problems, and [45] for regularization matrix models for stabilization at high-Reynolds numbers).

For second-order methods with overrelaxation, adequate second-order boundary conditions have to be developed. Without such conditions either additional dissipation or instabilities appear in boundary layers. The proposed schemes should now be put through the whole family of tests in order to find their place in the family of the LBM methods.

Recently, several approaches to stable LBM localized of high-Reynolds number flows on coarse grids have been reported [55,57,58]. Now it is necessary to understand better the mechanisms of the LBM subgrid properties, and to create the theory that allows us to prove the accuracy of LBM for under-resolved turbulence localized.

## ACKNOWLEDGMENTS

The preliminary version of this work [59] was widely discussed, and the authors are grateful to all the scientists who participated in this discussion. Special acknowledgments goes to V. Babu for comments relating to square-cylinder experiments, C. Care for discussion of positivity condition, H. Chen who forced us to check numerically the viscosity of the coupled steps model, S. Chikatamarla for providing the digitally extracted data used in Fig. 11, I.V. Karlin for deep discussion of results and background, S. Succi for very inspiring discussion and support, M. Geier, I. Ginzburg, G. Hazi, D. Kehrwald, M. Krafczyk, A. Louis, B. Shi, and A. Xiong who presented to us their related published, and sometimes unpublished, papers. This work is supported by Engineering and Physical Sciences Research Council (EPSRC) Grant No. GR/S95572/01.

- [1] S. Succi, *The Lattice Boltzmann Equation for Fluid Dynamics and Beyond* (Oxford University Press, New York, 2001).
- [2] P. L. Bhatnagar, E. P. Gross, and M. Krook, *Phys. Rev.* **94**, 511 (1954).
- [3] S. Chapman and T. Cowling, *Mathematical Theory of Non-Uniform Gases*, 3rd ed. (Cambridge University Press, Cambridge, 1970).
- [4] R. Benzi, S. Succi, and M. Vergassola, *Phys. Rep.* **222**, 145 (1992).
- [5] S. Chen and G. D. Doolen, *Annu. Rev. Fluid Mech.* **30**, 329 (1998).
- [6] F. Higuera, S. Succi, and R. Benzi, *Europhys. Lett.* **9**, 345 (1989).
- [7] I. V. Karlin, S. Ansumali, C. E. Frouzakis, and S. S. Chikatamarla, *Commun. Comput. Phys.* **1**, 616 (2006).
- [8] I. V. Karlin, S. S. Chikatamarla, and S. Ansumali, *Commun. Comput. Phys.* **2**, 196 (2007).
- [9] M. Junk, A. Klar, and L. S. Luo, *J. Comput. Phys.* **210**, 676 (2005).
- [10] A. Xiong, *Acta Mech. Sin.* **18**, 603 (2002).
- [11] P. Ehrenfest and T. Ehrenfest, *The Conceptual Foundations of the Statistical Approach in Mechanics* (Dover, New York, 1990).
- [12] A. N. Gorban, I. V. Karlin, H. C. Öttinger, and L. L. Tatarinova, *Phys. Rev. E* **63**, 066124 (2001).
- [13] A. N. Gorban, in *Model Reduction and Coarse-Graining Approaches for Multiscale Phenomena*, edited by A. N. Gorban, N. Kazantzis, I. G. Kevrekidis, H. C. Öttinger, and C. Theodoropoulos (Springer, Berlin, 2006), pp. 117–176; e-print cond-mat/0602024.
- [14] C. W. Hirt, *J. Comput. Phys.* **2**, 339 (1968).
- [15] Y. I. Shokin, *The Method of Differential Approximation* (Springer, New York, 1983).
- [16] A. N. Gorban, V. I. Bykov, and G. S. Yablonskii, *Essays on Chemical Relaxation* (Nauka Publications, Novosibirsk, 1986).
- [17] A. N. Gorban and I. V. Karlin, Institut des Hautes Études Scientifiques, Report No. IHES/P/03/57, 2003 (unpublished), e-print cond-mat/0308331.
- [18] A. N. Gorban and I. V. Karlin, *Invariant Manifolds for Physical and Chemical Kinetics*, Lecture Notes in Physics Vol. 660 (Springer, Berlin, 2005).
- [19] S. Ansumali, S. S. Chikatamarla, C. E. Frouzakis, and K. Boulouchos, *Int. J. Mod. Phys. C* **15**, 435 (2004).
- [20] G. Baskar and V. Babu, in *34th AIAA Fluid Dynamics Conference and Exhibit* (AIAA, Portland, OR, 2004), pp. 2004–2651.
- [21] H. Grad, *Commun. Pure Appl. Math.* **2**, 331 (1949).
- [22] X. Shan, X.-F. Yuan, and H. Chen, *J. Fluid Mech.* **550**, 413 (2006).
- [23] D. Jou, J. Casas-Vázquez, and G. Lebon, *Extended Irreversible Thermodynamics* (Springer, Berlin, 1993).
- [24] S. S. Chikatamarla and I. V. Karlin, *Phys. Rev. Lett.* **97**, 190601 (2006).
- [25] S. Succi, I. V. Karlin, and H. Chen, *Rev. Mod. Phys.* **74**, 1203 (2002).
- [26] A. J. Chorin, O. H. Hald, and R. Kupferman, *Physica D* **166**, 239 (2002).
- [27] J. D. Sterling and S. Chen, *J. Comput. Phys.* **123**, 196 (1996).
- [28] A. N. Gorban and I. V. Karlin, *Physica A* **206**, 401 (1994).
- [29] A. M. Lyapunov, *The General Problem of the Stability of Motion* (Taylor & Francis, London, 1992).
- [30] B. Robertson, *Phys. Rev.* **144**, 151 (1966).
- [31] B. M. Boghosian, J. Yepez, P. V. Coveney, and A. J. Wager, *Proc. R. Soc. London, Ser. A* **457**, 717 (2001).
- [32] I. V. Karlin, A. N. Gorban, S. Succi, and V. Boffi, *Phys. Rev. Lett.* **81**, 6 (1998).
- [33] X. He and L.-S. Luo, *Phys. Rev. E* **56**, 6811 (1997).
- [34] G. D. Birkhoff, *Dynamical Systems* (AMS Colloquium Publications, Providence, 1927).
- [35] V. I. Zubov, *Mathematical Theory of the Motion Stability* (Mobilnost Plus, St. Petersburg, 1997).
- [36] R. A. Brownlee, A. N. Gorban, and J. Levesley, *Phys. Rev. E* **74**, 037703 (2006).
- [37] F. Tosi, S. Ubertini, S. Succi, H. Chen, and I. V. Karlin, *Math. Comput. Simul.* **72**, 227 (2006).
- [38] R. A. Brownlee, A. N. Gorban, and J. Levesley, e-print cond-mat/0605359.
- [39] J. P. Boris and D. L. Book, *J. Comput. Phys.* **11**, 38 (1973).
- [40] D. L. Book, J. P. Boris, and K. Hain, *J. Comput. Phys.* **18**, 248 (1975).
- [41] E. F. Toro, *Riemann Solvers and Numerical Methods for Fluid Dynamics—a Practical Introduction* (Springer, Berlin, 1997).
- [42] *Flux-Corrected Transport. Principles, Algorithms, and Applications*, edited by D. Kuzmin, R. Lohner, and S. Turek (Springer, Berlin, 2005).
- [43] B. M. Boghosian, P. J. Love, and J. Yepez, *Philos. Trans. R. Soc. London, Ser. A* **362**, 1691 (2004).
- [44] S. Stolz and N. A. Adams, *Phys. Fluids* **11**, 1699 (1999).
- [45] J. Latt and B. Chopard, *Math. Comput. Simul.* **72**, 165 (2006).
- [46] P. J. Dellar, *J. Comput. Phys.* **190**, 351 (2003).
- [47] I. V. Karlin, A. Ferrante, and H. C. Öttinger, *Europhys. Lett.* **47**, 182 (1999).
- [48] S. Ansumali, I. V. Karlin, and H. C. Öttinger, *Europhys. Lett.* **63**, 798 (2003).
- [49] B. J. Vickery, *J. Fluid Mech.* **25**, 481 (1966).
- [50] R. W. Davis and E. F. Moore, *J. Fluid Mech.* **116**, 475 (1982).
- [51] A. Okajima, *J. Fluid Mech.* **123**, 379 (1982).
- [52] C. Cercignani, *Theory and Application of the Boltzmann Equation* (Scottish Academic Press, Edinburgh, 1975).
- [53] S. Ansumali and I. V. Karlin, *Phys. Rev. E* **66**, 026311 (2002).
- [54] D. d Humières, I. Ginzburg, M. Krafczyk, P. Lallemand, and L.-S. Luo, *Proc. R. Soc. London, Ser. A* **360**, 437 (2002).
- [55] R. Du, B. Shi, and X. Chen, *Phys. Lett. A* **359**, 564 (2006).
- [56] I. Rasin, S. Succi, and W. Miller, *J. Comput. Phys.* **206**, 453 (2005).
- [57] M. Geier, A. Greiner, and J. G. Korvink, *Phys. Rev. E* **73**, 066705 (2006).
- [58] I. V. Karlin, S. Ansumali, E. De Angelis, H. C. Öttinger, and S. Succi, e-print cond-mat/0306003.
- [59] R. A. Brownlee, A. N. Gorban, and J. Levesley, e-print cond-mat/0611444.
- [60] We are grateful to I. V. Karlin for this comment.